iScience

CellPress

Article

mCerulean3-Based Cameleon Sensor to Explore Mitochondrial Ca^{2+} Dynamics *In Vivo*

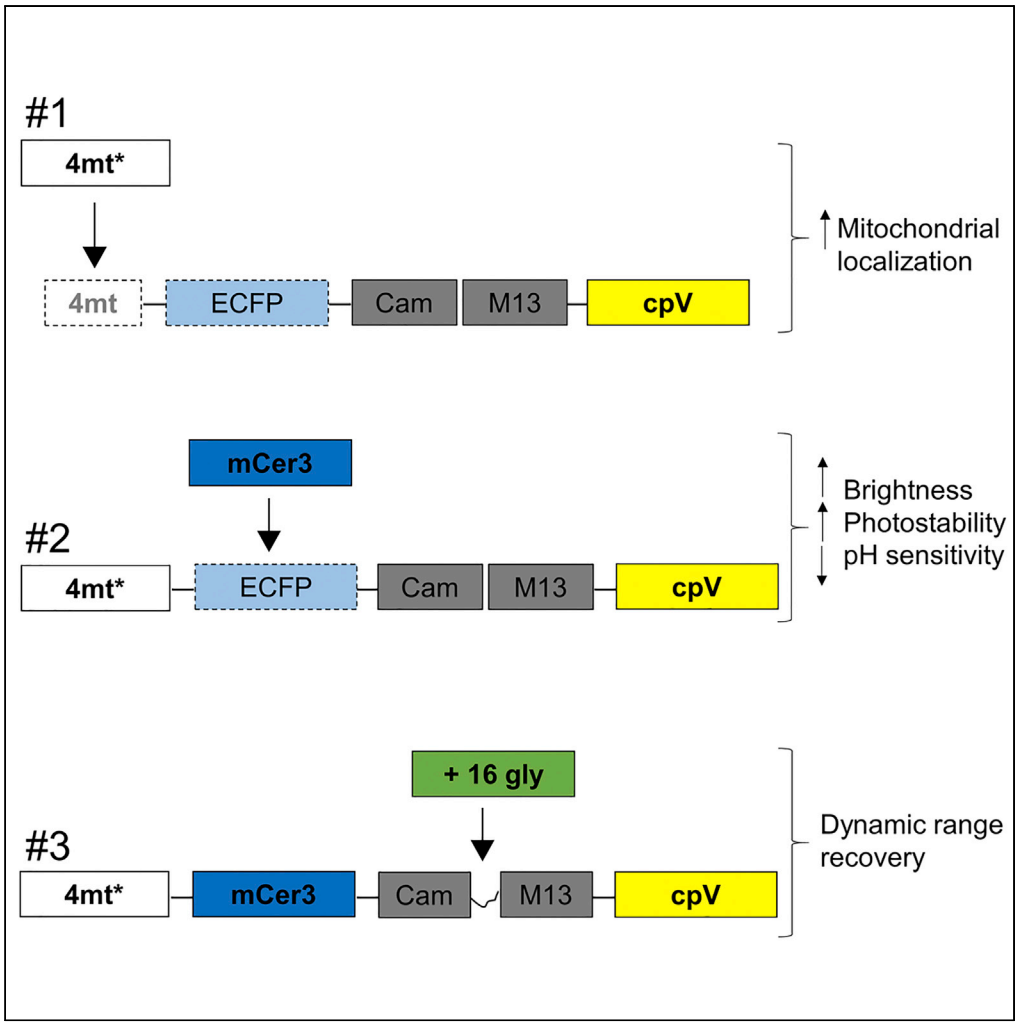

Elisa Greotti, Ilaria Fortunati, Diana Pendin, ..., Giorgio Carmignoto, Renato Bozio, Tullio Pozzan

tullio.pozzan@unipd.it

HIGHLIGHTS

Donor substitution in a mitochondrial Ca^{2+} sensor improves photo-physical properties

Mitochondria-targeting sequence amelioration enhances the sensor localization

Donor substitution allows FLIM-FRET analysis, with a compensation for pH bias

The performance of the sensor is improved *in situ*, *ex vivo*, and *in vivo*

Greotti et al., iScience *16*, 340–355
June 28, 2019
https://doi.org/10.1016/j.isci.2019.05.031

iScience

CellPress

Article

mCerulean3-Based Cameleon Sensor to Explore Mitochondrial Ca^{2+} Dynamics *In Vivo*

Elisa Greotti,[1,2] Ilaria Fortunati,[3] Diana Pendin,[1,2] Camilla Ferrante,[3] Luisa Galla,[1,2] Lorena Zentilin,[4] Mauro Giacca,[4] Nina Kaludercic,[1,2] Moises Di Sante,[2] Letizia Mariotti,[1,2,6] Annamaria Lia,[2] Marta Gómez-Gonzalo,[1,2] Michele Sessolo,[1,2,7] Giorgio Carmignoto,[1,2] Renato Bozio,[3] and Tullio Pozzan[1,2,5,8,*]

SUMMARY

Genetically Encoded Ca^{2+} Indicators (GECIs) are extensively used to study organelle Ca^{2+} homeostasis, although some available probes are still plagued by a number of problems, e.g., low fluorescence intensity, partial mistargeting, and pH sensitivity. Furthermore, in the most commonly used mitochondrial Förster Resonance Energy Transfer based-GECIs, the donor protein ECFP is characterized by a double exponential lifetime that complicates the fluorescence lifetime analysis. We have modified the cytosolic and mitochondria-targeted Cameleon GECIs by (1) substituting the donor ECFP with mCerulean3, a brighter and more stable fluorescent protein with a single exponential lifetime; (2) extensively modifying the constructs to improve targeting efficiency and fluorescence changes caused by Ca^{2+} binding; and (3) inserting the cDNAs into adeno-associated viral vectors for *in vivo* expression. The probes have been thoroughly characterized *in situ* by fluorescence microscopy and Fluorescence Lifetime Imaging Microscopy, and examples of their *ex vivo* and *in vivo* applications are described.

INTRODUCTION

The development of Genetically Encoded Indicators (GEIs) based on green fluorescent protein (GFP) mutants and their expression in cell subcompartments has revolutionized the study of intracellular signaling. Fluorescent proteins (FPs)-based GEIs can be divided into two major classes: single FP-based sensors and FRET-based indicators (see Pendin et al., 2017 for a recent review). Single FP-based GEIs are often characterized by high dynamic range (R_{max}/R_{min}), but they are generally "non-ratiometric," i.e., they respond to changes in their specific ligand concentration with changes in fluorescent intensities but not of their excitation or emission spectra. This characteristic makes the calibration of the changes in Ca^{2+} concentration ($[Ca^{2+}]$) *in situ* quite difficult for single fluorophore-based GECIs, and, more importantly, movement artifacts, occurring in some specimens, cannot be easily corrected. The FRET signal, on the contrary, is intrinsically ratiometric; changes in $[Ca^{2+}]$ are most commonly evaluated by recording the fluorescence intensity of both acceptor and donor FPs (exciting only the donor) and calculating their ratio (R). The vast majority of FRET-based sensors uses as the donor chromophore the cyan FP variant (CFP) and a yellow variant (YFP) as the acceptor. Among FRET-based sensors, the Ca^{2+}-sensitive probes Cameleons are the most used. The basic Cameleon structure is represented by CFP and YFP linked together by the Ca^{2+}-binding protein calmodulin and a calmodulin-binding domain from myosin light-chain kinase (M13). Many variants on this backbone have been produced over the last decade (Nagai et al., 2004; Palmer and Tsien, 2006; Horikawa et al., 2010). Surprisingly, the main stumbling blocks preventing the extensive use of Cameleons (and other FRET sensors based on CFP and YFP), i.e., the relatively low fluorescence quantum yield of the donor ECFP (Enhanced CFP), its complex kinetics, and strong tendency to photo-switch, have not been satisfactorily addressed. Recently, two CFP variants (mCerulean3 [Markwardt et al., 2011] and mTurquoise2 [Goedhart et al., 2010]) have been generated. These FPs are endowed with higher quantum yield, improved photostability, and decreased photo-switching behavior. Both these FPs are characterized by a single exponential decay rate, compared with the multiple components decay typical of CFP. The last feature makes these FPs particularly attractive for FLIM (Fluorescence Lifetime Imaging Microscopy) experiments.

As a model construct, we focused on the D3 Cameleon variant (D3cpv) because of its single and suitable affinity for Ca^{2+} (K_d) and its good R_{max}/R_{min} in response to Ca^{2+} changes. We thus substituted the ECFP with mCerulean3, and we extensively engineered the Cameleon cDNA developing a few approaches to modulate the features of CFP-YFP FRET-based sensors.

[1]Neuroscience Institute, National Research Council (CNR), 35131 Padua, Italy

[2]Department of Biomedical Sciences, University of Padua, 35131 Padua, Italy

[3]Department of Chemical Sciences and INSTM, University of Padua, 35131 Padua, Italy

[4]Molecular Medicine Laboratory, International Centre for Genetic Engineering and Biotechnology (ICGEB), 34149 Trieste, Italy

[5]Venetian Institute of Molecular Medicine (VIMM), 35131 Padua, Italy

[6]Present address: Division of Neurobiology, MRC Laboratory of Molecular Biology, CB2 0QH Cambridge, UK

[7]Present address: Aptuit an Evotec company, 37135 Verona, Italy

[8]Lead Contact

*Correspondence: tullio.pozzan@unipd.it

https://doi.org/10.1016/j.isci.2019.05.031

We thoroughly characterized the cytosolic and the mitochondria-targeted variant of mCerulean3-based Cameleon *in situ* using both intensity- and lifetime-based approaches. Finally, we inserted the mCerulean3-based probes into adeno-associated viral vectors (AAVs) to monitor cytoplasmic and mitochondrial Ca^{2+} dynamics *ex vivo*, in isolated neurons, in mature isolated cardiomyocytes, in acute slices from mouse brain, and *in vivo* in neurons of the somatosensory cortex.

RESULTS

Mitochondria-Targeted and Cytosolic mCerulean3-Based Cameleon Probes Optimization

We first focused on the modification of the mitochondria-targeted Cameleon, 4mtD3cpv, substituting the ECFP with mCerulean3 (Palmer et al., 2006) and generating the probe 4mtD3mCerulean3 (hereafter called 4mtD3mC3, Figure 1A) that was eventually transiently expressed in HeLa cells (Figure 1B). Filippin et al. previously showed a significant mislocalization of 4mtD3cpv to the cytosol (Filippin et al., 2005). We confirmed this result: indeed, analyzing the number of cells that display a mitochondrial localization of the sensors 24 h after transfection, we found that 4mtD3cpv was properly localized in the mitochondrial matrix in only 38.6% of the cells (Figure 1C). We thus redesigned the whole N terminus of the 4mtD3mC3 probe (see Transparent Methods for further details). This targeting sequence enabled proper mitochondrial cleavage (Figure 1D) and localization (87.5% of cells after 24 h and ≅100% after 72 h, Figure 1C). To check whether mCerulean3 brightness improvement, reported for the cytosolic version of the protein (Markwardt et al., 2011), was maintained in the complex contest of a Cameleon probe expressed in a different environment, the mitochondrial matrix, the fluorescent intensity at 480 nm (the peak emission wavelength of the donor) in HeLa cells transfected with 4mtD3cpv or 4mtD3mC3 was measured. Since FRET efficiency is very similar in the two probes (see Figure 2B), the fluorescence intensity of cpV emission (excited at 512 nm, emission 535 nm), present in both probes, was used to normalize for the protein expression level (see Transparent Methods). The fluorescence mean intensity in 4mtD3mC3 expressing cells was about 42% higher than that of cells expressing 4mtD3cpv (Figure 1E).

In ratiometric GECIs, a key parameter for their practical use is the value of R_{max}/R_{min} *in situ*. To this end, HeLa cells have been permeabilized to obtain accurate minimal and maximal Ca^{2+} levels thanks to the equilibration between the perfused saline and the mitochondrial matrix (see Transparent Methods). The substitution of the ECFP with mCerulean3 caused a reduction (about 20%) in R_{max}/R_{min} of 4mtD3mC3 (R_{max}/R_{min} = 1.94, Table 1) compared with 4mtD3cpv (R_{max}/R_{min} = 2.44, Table 1). We first attempted to substitute the acceptor FP (Nagai et al., 2004), replacing cpV with other YFP variants, Citrine or YPet, but none of them allowed a recovery of R_{max}/R_{min} (data not shown). Finally, we increased the linker flexibility between the two Ca^{2+} responsive elements, by including poly-Gly linkers of different lengths, from 2 to 16 (Chichili et al., 2013). The addition of a 16-amino acid poly-Gly allowed the complete recovery of the R_{max}/R_{min}, increasing it to 2.37 (Figure 1F and Table 1). The ability of the newly generated variant (called 4mtD3mC3+16) to report changes in mitochondrial $[Ca^{2+}]$, compared with the other two probes, was finally tested and confirmed in intact cells (Figure 1G). Furthermore, the increased signal to noise ratio has been exploited to monitor the dynamics of $[Ca^{2+}]$ in single mitochondria upon stimulation with histamine (Figure 1H and Video S1).

These promising results were exploited to generate a mCerulean3-based cytosolic Cameleon. ECFP was thus substituted with mCerulean3 in D3cpv sensor, and the glycine-linkers were added between the two Ca^{2+} responsive elements, obtaining the probe D3mC3+16 (Figure 1I). The cytosolic localization of the probe was confirmed using fluorescence microscopy (Figure 1J). The ability of the probes to detect cytosolic Ca^{2+} ($[Ca^{2+}]_c$) changes upon histamine stimulation (Figure 1K) and the improvement in mCerulean3 fluorescence compared with ECFP (Figure 1L) were confirmed.

Since the classical digitonin treatment (as used earlier) causes a rapid probe leakage into the medium, to measure the R_{max}/R_{min} of the cytosolic probes, we employed a very low dose of digitonin (Hofer et al., 1998, see Transparent Methods), a protocol that prevents probe leakage. Despite the addition of 16 Gly, the D3mC3+16 shows a significant reduction of the R_{max}/R_{min} ratio (Figure 1M) compared with the original probe.

Photostability and pH Effect

Photostability is an important factor in experiments requiring prolonged imaging of living cells. Photobleaching of mCerulean3 has been shown to be significantly less than that of ECFP (Markwardt

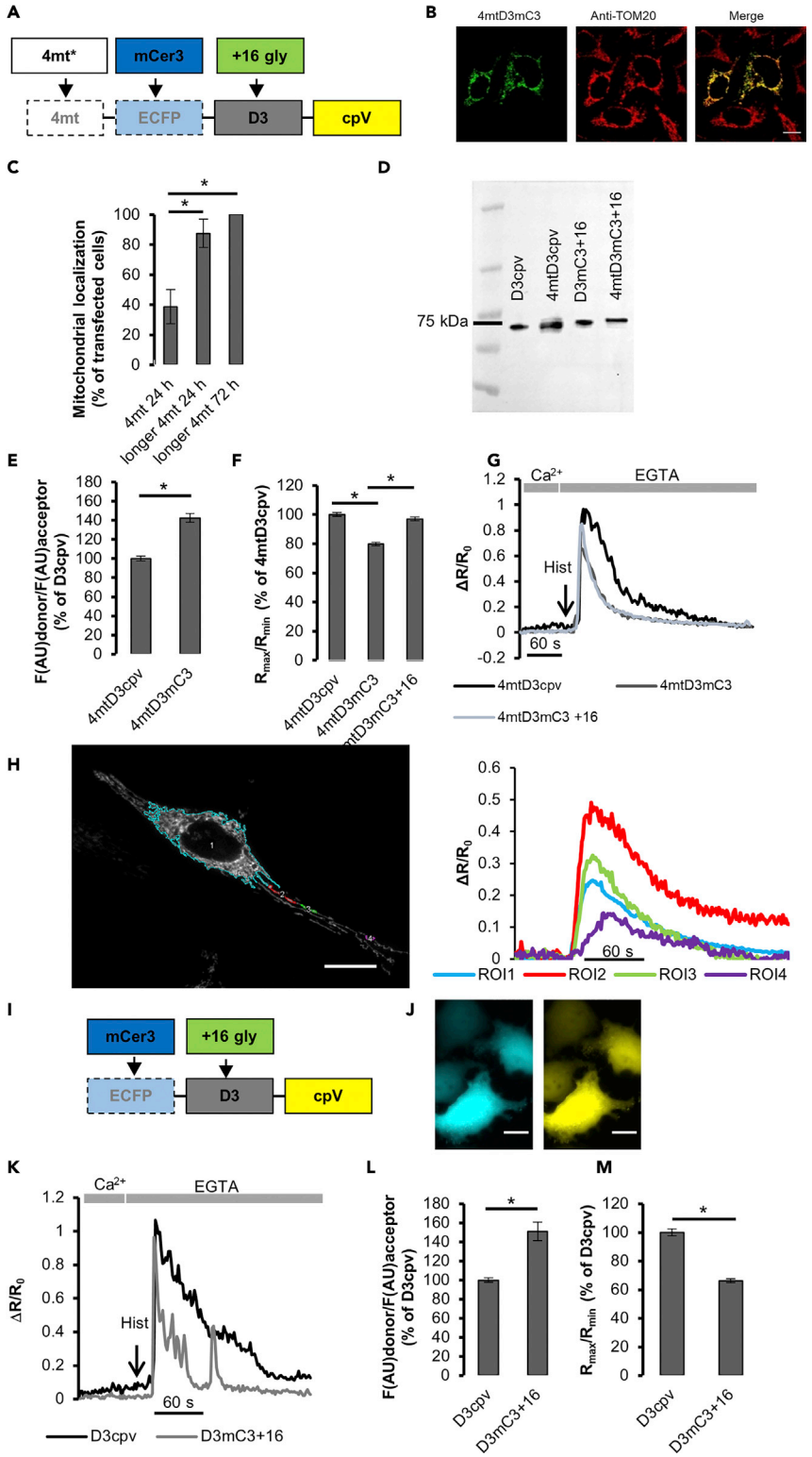

Figure 1. Optimization of Mitochondrial and Cytosolic Cameleons

(A–D) *Cloning and localization of the mitochondrial probe.* (A) Schematic representation of the cloning strategy used to modify the mitochondria targeting sequence (4mt) with the elongated version (4mt*) and to substitute ECFP with mCerulean3 in 4mtD3cpv Cameleon probes. (B) Confocal images of 4mtD3mC3. The mitochondrial localization of the

Figure 1. *Continued*

probe was evaluated as the co-localization with a mitochondrial marker, TOM20. Yellow color indicates co-localization of the mitochondrial maker and 4mtD3mC3. Scale bar, 10 μm. (C) The bar chart represents the mean ± SEM of the number of cells (N) showing a proper mitochondrial localization, normalized to the number of transfected cells for each field. N ≥ 17 cells for each condition. (D) Mitochondria-targeting sequence cleavage. Twenty-four hours after transfection, total proteins were extracted and subjected to Western blot analysis with antibodies anti-GFP. (E–H) *The newly generated mitochondrial mCerulean3-based Cameleon is a functional and brighter probe compared with the original 4mtD3cpv*. (E) The bar chart represents the mean ± SEM of ECFP and mCerulean3 fluorescence normalized to cpV fluorescence, in HeLa cells expressing mitochondrial Cameleon probes. N ≥ 39 cells for each condition. (F) The bar chart shows the R_{max}/R_{min} of the mitochondrial probes as mean ± SEM (normalized to 4mtD3cpv) of N ≥ 24 cells for each condition. (G) Representative kinetics of mitochondrial Ca^{2+} uptake in HeLa cells expressing 4mtD3cpv (black), 4mtD3mC3 (gray) and 4mtD3mC3+16 (light gray). HeLa cells transiently transfected with 4mtD3cpv, 4mtD3mC3, or 4mtD3mC3+16 were treated with 100 μM histamine (Hist) and perfused with 600 μM EGTA where indicated. (H) *Left*. Image of HeLa cells expressing 4mtD3mC3+16 along with the analyzed ROIs. *Right*. Representative kinetics of single mitochondrial Ca^{2+} uptake analysis in HeLa cells expressing 4mtD3mC3+16, using the protocol described for panel G. Data are plotted as $\Delta R/R_0$ as defined in the Transparent Methods section. (I–M) *Cloning and localization of the mitochondrial probe*.

(I) Schematic representation of the cloning strategy used to substitute ECFP with mCerulean3 in D3cpv Cameleon probes. (J) Fluorescence microscope image of the donor (cyan) and the acceptor (yellow) cytosolic D3mC3. Scale bar, 10 μm. (K–M) *The newly generated mCerulean3-based Cameleon is a functional and brighter probe compared with the original D3cpv*. (K) Representative kinetics of cytosolic Ca^{2+} uptake in HeLa cells expressing D3cpv or D3mC3+16 employing the same protocol as in panel A. Data are presented $\Delta R/R_0$. (L) The bar chart represents the mean ± SEM of ECFP and mCerulean3 fluorescence, normalized to cpV fluorescence, in HeLa cells expressing cytosolic Cameleon probes. N ≥ 27 cells for each condition. (M) The bar chart shows the R_{max}/R_{min} of the cytosolic probes as mean ± SEM (normalized to D3cpv) of N ≥ 18 cells for each condition. Statistical significance (*$p < 0.05$) was detected by Wilcoxon test for comparison between two groups and by one-way ANOVA and Bonferroni post hoc for comparison among three different groups. See also Figure S1 and Table S7.

et al., 2011), but the effect of this property in an FRET sensor such as Cameleon is difficult to predict (see Transparent Methods for further details). HeLa cells expressing the ECFP-based or mCerulean3-based Cameleons were thus imaged for 20 min with the same settings for both illumination and acquisition. R was monitored in conditions of basal [Ca^{2+}] or in the absence of Ca^{2+} in the medium and cytosolic [Ca^{2+}] clamped at very low levels (see Transparent Methods). Figure S1A shows time-dependent R changes at basal [Ca^{2+}] in representative cells (data quantification is provided in Figure S1B). The decrease of R is faster (about twofold) in D3cpv-expressing cells compared with cells expressing either D3mC3 or D3mC3+16. A similar difference was observed in cells in the absence of external Ca^{2+} (i.e., employing a Ca^{2+} clamp method, see Transparent Methods; Figures S1C and S1D) and for the mitochondria-targeted Cameleon probes (Figures S1E and S1F for basal FRET photostability and Figures S1G and S1H for minimal FRET photostability). Given the much better performance of mCerulean3-based Cameleons in the presence of 16 glycines, most of the following data were performed using only these constructs.

Last, since variations in pH can affect several GECI properties, depending on single FPs pK_a (Koldenkova and Nagai, 2013), we also investigated this issue in HeLa cells transiently expressing the cytosolic or the mitochondrial Cameleons, by imposing the different pH that can be experienced by these two compartments in live cells. We found that, as predicted by the mCerulean3 pK_a, the sensors based on this protein are much less sensitive to pH changes (see Table 1 and Figures S1I–S1P for further details).

Ca^{2+} Affinity

The profound structural changes introduced in the probes may also affect their affinity for Ca^{2+} (Horikawa et al., 2010). The *in situ* calibration of the Ca^{2+} affinity was thus carried out for the ECFP- and mCerulean3-based mitochondria-targeted probes, using the passive Ca^{2+} loading procedure in digitonin-permeabilized cells (Figures 2A, Filippin et al., 2005). The experimentally calculated K_d *in situ* (at the physiological matrix pH 8.0) is lower for 4mtD3cpv (K_d = 3.2 ± 0.9 μM) (Table 1, Figure 2B, black trace) compared with that of 4mtD3mC3+16 (K_d = 6.2 ± 0.99 μM) (Table 1, Figure 2B, red trace). The *in situ* calibration has been performed also for the cytosolic probes. The estimated K_d *in situ* was 1.8 ± 0.5 μM for D3cpv (Table 1, Figure 2C, black trace) and 4.1 ± 1.1 μM for D3mC3+16 (Table 1, Figure 2C, red trace).

We then exploited the calculated K_d to measure the peak of $[Ca^{2+}]_m$, reached in the mitochondrial matrix, upon ER Ca^{2+} release induced by IP_3R (Inositol trisphosphate receptor) stimulation. $[Ca^{2+}]_m$ peaks, elicited

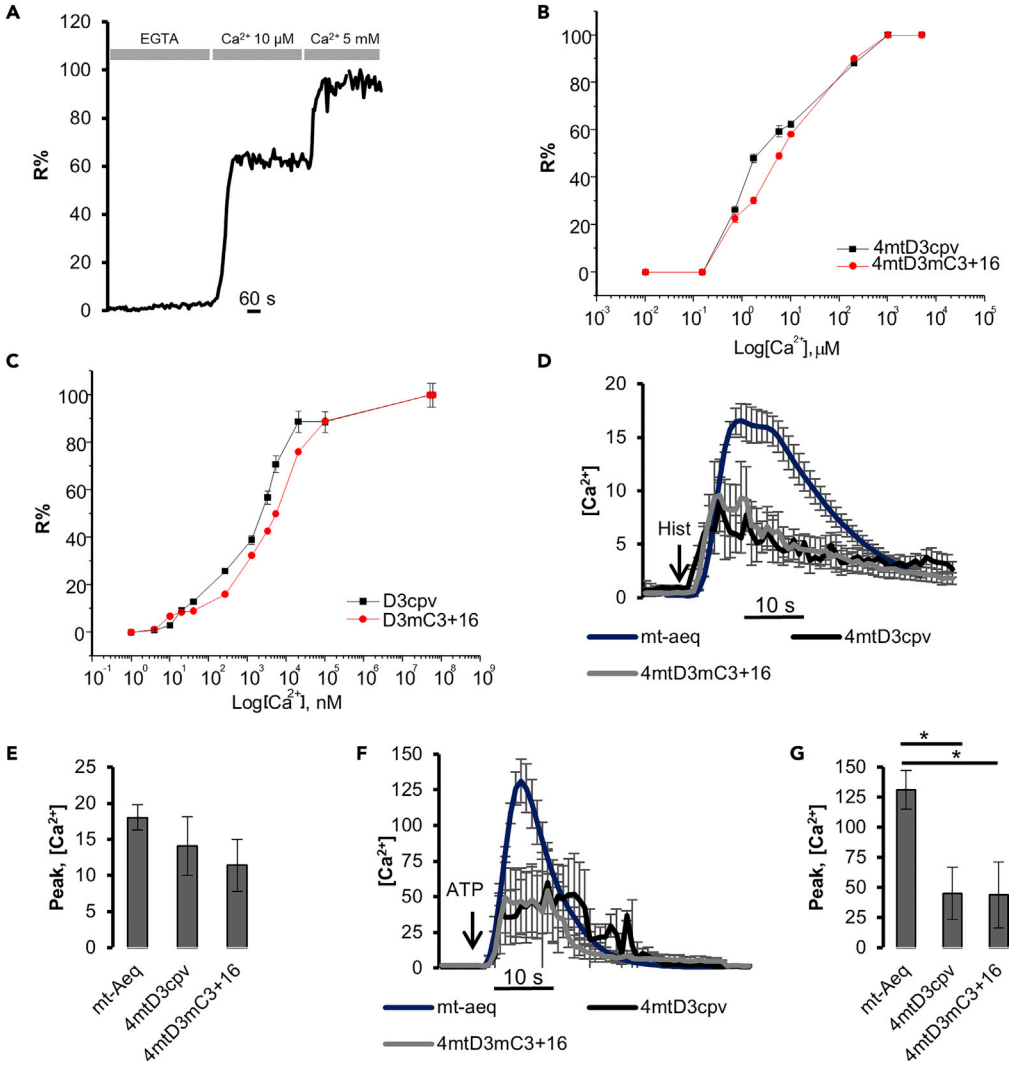

Figure 2. Ca^{2+} Affinity and Mitochondrial Ca^{2+} Uptake upon Stimulation

(A–C) *Titration protocol*. (A) Representative kinetics of R% in permeabilized HeLa cells transiently expressing the 4mtD3cpv. Where indicated, digitonin-permeabilized cells were perfused with an intracellular-like medium without energy sources and containing different [Ca^{2+}] together with 5 µM of the mitochondrial uncoupler, FCCP. In the representative trace 10 µM $CaCl_2$ was perfused; 5 mM $CaCl_2$ was finally added to reach the maximal FRET. (B and C) *In situ* Ca^{2+} titration mCerulean3-based Cameleon (red trace) or original Cameleon (black trace). The graph represents the data as mean ± SEM of N ≥ 5 cells for each [Ca^{2+}], at pH 8.0 for mitochondrial (B) and at pH 7 for cytosolic probes (C).

(D–G) *Stimulated mitochondrial Ca^{2+} uptake*. Average kinetics of mitochondrial Ca^{2+} uptake in HeLa (D) or MEFs (F) cells expressing 4mtD3mC3+16 (gray trace), 4mtD3cpv (black trace), or mt-Aequorin (mt-aeq, blue trace) employing the same protocol as in Figure 1G, with the only exception to MEFs, stimulated with ATP, 100 µM. Data are presented as [Ca^{2+}], mean ± SEM. The bar chart shows the average of the mitochondrial Ca^{2+} peaks elicited by histamine application in HeLa cells (E) and ATP application in MEF cells (G) as mean ± SEM of N ≥ 18 and 7 cells, respectively, for each condition. Statistical significance (*$p < 0.05$) was detected by one-way ANOVA and Bonferroni post hoc.

by histamine, were measured in a selected low responding HeLa cell batch (Figures 2D and 2E) and by ATP in a strongly responding MEF (Mouse Embryonic Fibroblast) cell line (Figures 2F and 2G) and compared with the values measured with targeted aequorin. In HeLa cells, the mean [Ca^{2+}] peak in mitochondria was 18 µM, as measured with aequorin, while those measured with mitochondrial targeted Cameleons were on average 11 µM and 14 µM for 4mtD3mC3+16 and 4mtD3cpv, respectively (Figure 2E). In some cells (9% and 29% of cells expressing 4mtD3mC3+16 and 4mtD3cpv, respectively), the R values of the peaks

		pH 7.0	pH 8.0
4mtD3mC3+16	K_d (μM)	6.48 ± 0.81	6.18 ± 0.99
	N	1.07 ± 0.13	0.72 ± 0.07
	R_{max}/R_{min}	1.92 ± 0.03	2.37 ± 0.03
4mtD3cpv	K_d (μM)	2.49 ± 0.23	3.22 ± 0.86
	N	0.99 ± 0.09	0.68 ± 0.11
	R_{max}/R_{min}	2.48 ± 0.13	2.44 ± 0.03
D3mC3+16	K_d (μM)	4.15 ± 1.12	
	N	0.77 ± 0.12	
	R_{max}/R_{min}	3.48 ± 0.07	
D3cpv	K_d (μM)	1.83 ± 0.55	
	N	0.68 ± 0.14	
	R_{max}/R_{min}	5.36 ± 0.13	

Table 1. *In Situ* Properties of Cameleon Probes

K_d, dissociation constant; n, Hill constant; R_{max}/R_{min}, dynamic range. The K_d and R_{max}/R_{min} values have been compared for pH values (7.0 and 8.0) that can be observed in the mitochondrial matrix in different experimental conditions (pH 7.0 in Figure S1I, related to Figure 1). The estimated Ca^{2+} affinities vary by about 5% at pH 7.0 compared with those at pH 8.0 for the 4mtD3mC3+16 probe and by about 20% for the 4mtD3cpv, indicating that the substitution of the donor decreases significantly the pH sensitivity of the mitochondrial probe. The acidification from pH 8.0 to 7.0 results also in a significant change of R_{max}/R_{min} in both 4mtD3cpv and 4mtD3mC3+16. Data are presented as mean ± SEM of $N \geq 5$ (number of cells).

were so close to R_{max} that the calculation of the $[Ca^{2+}]$ in the matrix was prone to major errors. For this reason, those cells have been excluded from the analysis.

In MEF cells, stimulated with ATP, the mean Ca^{2+} peaks measured with aequorin were about 131 μM, i.e., much higher than those reported by the two Cameleons (44 and 45 μM for 4mtD3mC3+16 and 4mtD3cpv, respectively). Also in this latter case, as explained before, 20% and 40% of cells expressing 4mtD3mC3+16 and 4mtD3cpv, respectively, were very close to R_{max}, and thus they were not included in the means.

FRET Efficiency Evaluation and pH Sensitivity with FLIM

To evaluate FRET efficiency, two methods are usually employed: the intensity-based (mostly using the acceptor photobleaching approach) or fluorescence lifetime-based measurements. FLIM measurements, compared with intensity-based images, have the advantage of being mostly independent of fluorophore concentration, excitation intensity fluctuation, sample thickness, or photobleaching (Marcu et al., 2014). Thus, analysis based on a time-resolved technique has often been employed to precisely estimate FRET efficiency. Usually, in FLIM-FRET measurements, energy transfer is observed as a decrease of the donor fluorescence lifetime. To calculate FRET efficiency under different conditions (see Transparent Methods), it is first necessary to determine the lifetime of the donor only. To this end, HeLa cells were transfected with ECFP or mCerulean3 targeted to the mitochondrial matrix. As previously reported, the fluorescence decay of ECFP can be fitted by a two-exponential terms model (Millington et al., 2007), whereas the mCerulean3 decay is mono-exponential (Markwardt et al., 2011) (Table S1 and Figures S2A and S2B). Next, applying the same Ca^{2+} titration protocol described for the intensity-based approach, we evaluated FRET efficiency in HeLa cells expressing 4mtD3cpv or 4mtD3mC3+16. The lifetime of 4mtD3cpv can be fitted by either a double or a triple exponential model, whereas in the other probe, the lifetime can be fitted with a double exponential model, where only the second shorter donor lifetime is associated to the FRET process. Given the low accuracy of a triple exponential fitting, a double exponential fitting model has been used also in the case of 4mtD3cpv (Geiger et al., 2012). For both sensors, the shorter donor lifetime component is clearly dependent on $[Ca^{2+}]$, whereas the longer donor lifetime is less affected by the Ca^{2+} levels (Table S2 for 4mtD3mC3+16 and Table S3 for 4mtD3cpv). At maximum $[Ca^{2+}]$, FRET efficiency was 43% in the case of 4mtD3cpv (Table 2 and Figure 3A) and 36% for 4mtD3mC3+16 (Table 2 and

Sample	τ_1 (ns)	A_1	τ_2 (ns)	A_2	$<\tau>$	E_{FRET}
4MTD3CPV PH = 8, CA_{MIN}	2.89 ± 0.02	49 ± 1%	0.88 ± 0.02	51 ± 1%	1.86 ± 0.01	31%
4MTD3CPV PH = 8, CA_{SAT}	2.66 ± 0.02	41 ± 1%	0.73 ± 0.01	59 ± 1%	1.53 ± 0.02	43%
4MTD3CPV PH = 7.5, CA_{MIN}	2.84 ± 0.01	44 ± 1%	0.75 ± 0.02	56 ± 1%	1.68 ± 0.02	32%
4MTD3CPV PH = 7.5, CA_{SAT}	2.75 ± 0.02	43 ± 1%	0.71 ± 0.02	57 ± 1%	1.58 ± 0.02	36%
4MTD3MC3+16 PH = 8, CA_{MIN}	3.58 ± 0.03	72 ± 1%	1.24 ± 0.05	28 ± 1%	2.94 ± 0.01	18%
4MTD3MC3+16 PH = 8, CA_{SAT}	3.21 ± 0.05	65 ± 1%	0.63 ± 0.05	35 ± 1%	2.31 ± 0.06	36%
4MTD3MC3+16 PH = 7.5, CA_{MIN}	3.55 ± 0.03	61 ± 1%	0.94 ± 0.03	39 ± 1%	2.53 ± 0.03	25%
4MTD3MC3+16 PH = 7.5, CA_{SAT}	3.39 ± 0.03	60 ± 2%	0.75 ± 0.03	40 ± 2%	2.34 ± 0.08	30%

Table 2. Decay Fitting Parameters of Cells Expressing 4mtD3cpv and 4mtD3mC3+16 at pH Equal to 8.0 or 7.5

$Ca^{2+}{}_{min}$ and $Ca^{2+}{}_{sat}$ are, respectively, the minimum and the saturation Ca^{2+} concentrations (500 μM). τ_i are the lifetimes, A_i are the relative amplitudes, and average lifetimes ($<\tau>$) are the amplitude-weighted lifetimes. Data are reported as mean ± SEM of N ≥ 5 cells for each [Ca^{2+}] and pH condition. See also Tables S1–S5.

Figure 3B), whereas in the absence of Ca^{2+} the FRET efficiencies decrease to 31% (Table 2 and Figure 3A) and 18% (Table 2 and Figure 3B) respectively. Thus, the dynamic range, estimated as the ratio between maximal and minimal FRET efficiencies at pH 8.0, is 2 for 4mtD3mC3+16 and 1.4 for 4mtD3cpv (Figures 3A and 3B and Table 2).

Since we found that R is affected by pH (see Figures S1I–S1P and Table 1) and previous studies have demonstrated that pH has a significant impact on ECFP lifetime (Villoing et al., 2008), we carried out FLIM-based analysis of 4mtD3cpv and 4mtD3mC3+16 at different [Ca^{2+}] and different pH. We found a decrease in the dynamic range of both probes upon acidification (see Figure S2). Furthermore, we found that lifetime analysis allows the discrimination between pH and Ca^{2+} effect, employing the rise term analysis (Borst et al., 2008). The rise term reflects the delay in acceptor emission decay due to indirect excitation from donor emission, and it is represented by a negative amplitude contribution to the acceptor emission decay. Upon mitochondrial matrix acidification, the disappearance of this rise term in the acceptor channel occurs independently of changes in [Ca^{2+}] (see Figures S2E and S2F and Tables S4 and S5 for further details).

FLIM Analysis Reveals Mitochondrial [Ca^{2+}] Heterogeneity in Resting Condition

The FLIM approach has been finally applied (using only the 4mtD3mC3+16) to estimate the resting Ca^{2+} level in the mitochondrial matrix in different conditions: naive cells, cells overexpressing the mitochondrial Ca^{2+} uniporter (MCU), the MCU modulator MICU1, or both proteins. The first observation is that, under resting conditions, the FLIM maps reveal a substantial heterogeneity of mitochondria in terms of [Ca^{2+}] (Figure 3C), possibly because of constitutive transfer of Ca^{2+} from the ER to some mitochondria (those located near the mouth of IP_3R) (Cárdenas et al., 2010). As expected (Csordas et al., 2013; Mallilankaraman et al., 2012; Patron et al., 2014), overexpression of MCU alone or MCU and MICU1 decreased the donor lifetime (Figure 3D), indicating the predicted increase in $[Ca^{2+}]_m$. Surprisingly, also the overexpression of only MICU1 caused a small reduction of donor lifetime. A small increase in the $[Ca^{2+}]_m$ upon MICU1 overexpression has been previously reported employing GCaMP family Ca^{2+} sensors (Csordas et al., 2013; Mallilankaraman et al., 2012; Patron et al., 2014). We did not observe such an increase employing 4mtD3mC3+16 using the intensity-based approach (Figure 3E), possibly due to the lower K_d for Ca^{2+} of the Cameleon compared with GCaMP sensors. Given the similar effect of acidification and Ca^{2+} increase on donor lifetime, we investigated whether a reduction in matrix pH could contribute to the shorter lifetime observed in MICU1-overexpressing cells. Indeed, the rise term analysis suggested a decrease in matrix pH in cells overexpressing MICU1 (Table S6). We thus directly verified whether overexpression of MICU1 induces changes in the matrix pH by using the GEI mt-SypHer (Poburko and Demaurex, 2012). A significant decrease in matrix pH from 7.7 in control cells to 7.5 in cells overexpressing MICU1 and/or MCU was observed (Figure 3F). We thus repeated FLIM analysis including only cells that presented an acceptor rise (Figures 3G and S2C, Table S6). In these cells, MICU1 overexpression causes a marginal, non-significant

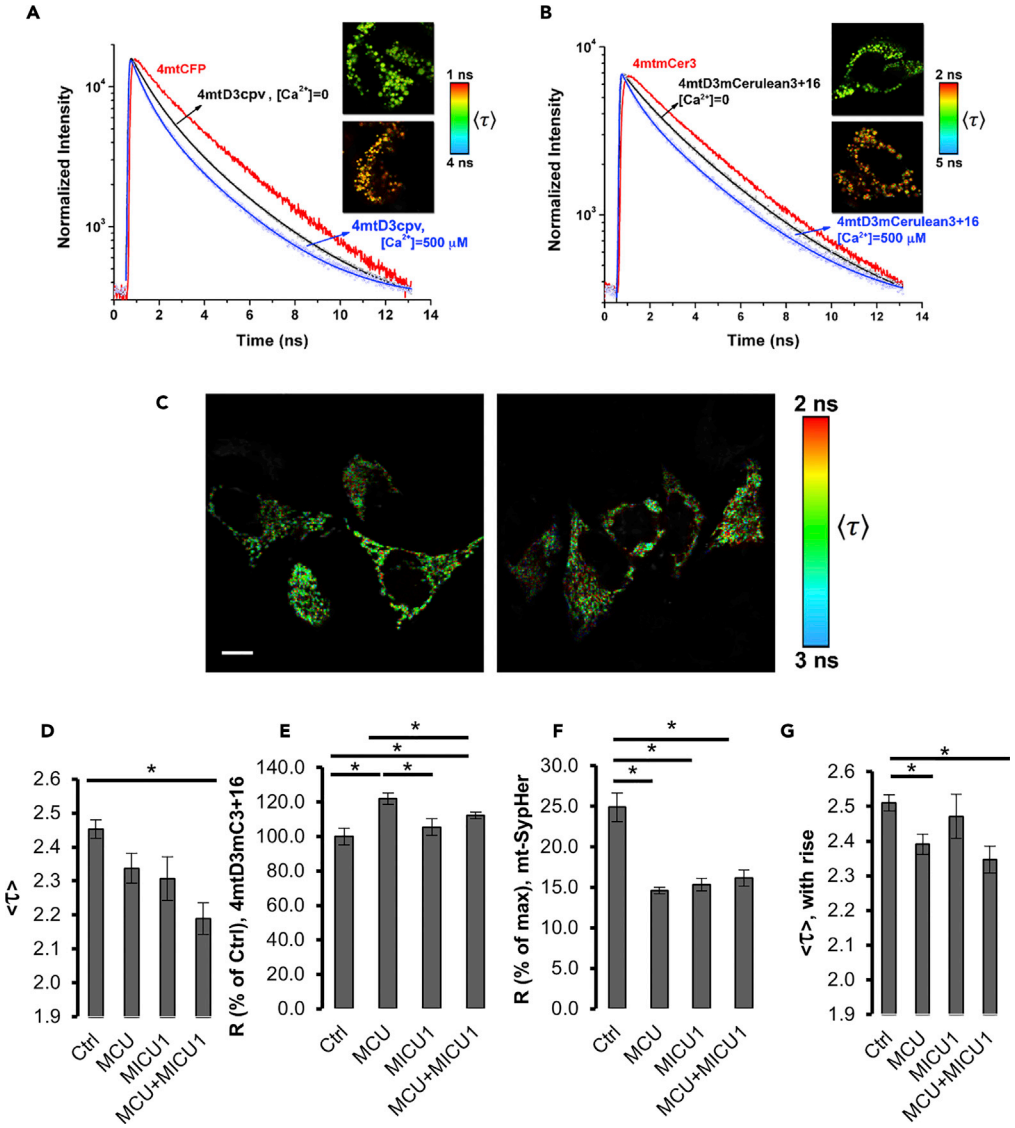

Figure 3. FLIM Analysis of FRET Efficiency and Alterations in MCUC Components Protein Level Effect on Mitochondria [Ca^{2+}] in Resting Conditions

(A) Normalized fluorescence decay of 4mtD3cpv at minimum FRET (black squares) and maximum FRET (blue dots). The full lines are the fitting curves with a two-exponential model. For comparison, the decays of 4mt-CFP expressed in mitochondria are reported (red lines). The insets are the false-color FLIM images (amplitude-weighted lifetime) at minimum and maximum FRET, in the 1- to 4-ns range. Data are from N ≥ 15 cells for each condition.

(B) Normalized fluorescence decay of 4mtD3mC3+16 at minimum FRET (black squares) and maximum FRET (blue dots). The full lines are the fitting curves with a two-exponential model. For comparison, the decay of mCerulean3 expressed in mitochondria is reported (red line, one-exponential fitting model). The insets are the false-color FLIM images (amplitude-weighted lifetime) at minimum and maximum FRET, in the 2- to 5-ns range. Data are from N ≥ 15 cells for each condition.

(C) FLIM images of 4mtD3mC3+16 in intact HeLa cells in resting conditions. FLIM images report the amplitude-weighted lifetime in the 2- to 3-ns range. Scale bar, 10 μm.

(D) The bar chart represents the <τ> mean ± SEM of N ≥ 27 cells expressing 4mtD3mC3+16 and overexpressing MCU, MICU1, or MCU and MICU1.

(E) The bar chart represents the mean ± SEM of the R (cpV/mCerulean3), normalized to control, of N ≥ 25 cells expressing 4mtD3mC3+16 and overexpressing MCU, MICU1, or both.

(F) The bar chart represents the mean ± SEM of R (% of max, where maximum is the R at pH 9.0) of N ≥ 13 cells transfected with mt-SypHer in the presence of void vector, MCU, MICU1, or MCU and MICU1.

Figure 3. *Continued*
(G) The bar chart represents the <τ> mean ± SEM of N ≥ 15 cells expressing 4mtD3mC3+16 and overexpressing MCU, MICU1, or MCU and MICU1, including only data that display the negative rise term in the acceptor channel.
See also Figure S2 and Tables S1–S6.

increase in matrix [Ca^{2+}], whereas MCU (overexpressed alone or together with MICU1) induces a much larger [Ca^{2+}] rise.

In Vivo Delivery of the Generated Probes in Mice

To express mCerulean3-based Cameleons *in vivo*, adeno-associated viruses (AAVs) were generated with capsid serotype 9 (Bish et al., 2008; Pacak et al., 2006; Foust et al., 2009). AAV9-CMV-D3mC3+16 or AAV9-CMV-4mtD3mC3+16 was first tested in cultured neonatal rat cardiomyocytes. Ninety-six hours after transfection, spontaneous cytosolic and mitochondrial Ca^{2+} oscillations were observed with both probes (Figures 4A and 4B, respectively). Of note, the cytosolic peaks displayed a larger change in $\Delta R/R_0$ compared with the mitochondrial ones. Figure S3 shows one of the advantages of a ratiometric probe such as 4mtD3mC3+16 compared with one of the brightest "non-ratiometric" sensors available, mtGCaMP6f (Mammucari et al., 2015; Tosatto et al., 2016). The response of the ratiometric probe nicely corrects for the substantial movement artifact due to contraction in all transfected cells. Although in many cells the mtGCaMP6f appears to nicely report the mitochondrial Ca^{2+} increases during spontaneous beating (Figure S3A), in others (Figure S3B) the changes in fluorescence are minimal and hardly distinguishable from the changes in focus due to contraction observed in cells solely transfected with a mitochondrial GFP (Figure S3C).

AAV9-CMV-D3mC3+16 or AAV9-CMV-4mtD3mC3+16 was then used to infect adult cardiac cells in mice via tail vein injection. Six months after the infection, cardiomyocytes were isolated. Figure 4 shows the typical kinetics of cytosolic and mitochondrial Ca^{2+} changes due to spontaneous Ca^{2+} oscillations (Figures 4C and 4D, respectively) or induced by the application of caffeine (Figures 4E and 4F, respectively). Noteworthy, the amplitude of mitochondrial Ca^{2+} rise (in terms of $\Delta R/R_0$) was larger in adult cardiomyocytes compared with that in neonatal cells.

The different heart-beating rate among different animals, which inversely correlate with body weight (Ostergaard et al., 2010), raises the question of the suitability of these probes in models that can contribute to the study of human cardiac pathophysiology. To address this issue, we exploit the transduction of AAV9-CMV-D3mC3+16 or AAV9-CMV-4mtD3mC3+16 in human induced pluripotent stem cell-derived cardiomyocytes. In Figures 4G and 4H, we show that both cytosolic and mitochondrial mCerulean3-based Cameleons were able to report spontaneous and synchronous (among cells of the same coverslips) Ca^{2+} oscillations at a beating frequency similar to that of human beings.

To specifically express the probes in neurons of mouse brain, the CMV promoter was substituted with the neuronal-specific promoter synapsin 1 (Kugler et al., 2001). The AAVs were first tested in cultures of primary neonatal cortical neuron (typically contaminated by non-neuronal cells) where the exclusive neuronal expression and the proper localization of both probes have been tested (see Figure S4). Furthermore, we exploit cultured neurons to test the ability of both probes to detect spontaneous activity (see Figures S5A and S5B), Ca^{2+} changes in response to a depolarizing stimulation (see Figures S5C and S5D), or the fast Ca^{2+} spikes elicited by the GABA-A antagonist picrotoxin (see Figures S5E–S5H).

AAV9-syn-D3mC3+16 or AAV9-syn-4mtD3mC3+16 was then injected intracranially in 1-month old mice, and the cytosolic and mitochondrial Ca^{2+} levels were tested in acute hippocampal slices 2 weeks post infection. The neuronal specificity and the correct subcellular localization were verified *ex vivo* (see Figure S6). In the hippocampal slices, a larger increase in mitochondrial Ca^{2+} (recorded at the two-photon microscope; see Figures S7A and S7B for spectra characterization), compared with that of the cytosol, was observed upon stimulation with group I metabotropic glutamate receptor agonist ((*S*)-3,5-Dihydroxyphenylglycine, DHPG, 50 μM) (Figures 5A and 5B). DHPG response can be detected as a single Ca^{2+} rise (as shown in Figure 5A, cytosol, and 5B, mitochondria),or it can generate an oscillatory pattern (Figures 5C, cytosol, and 5D, mitochondria). However, in the mitochondria the oscillations of [Ca^{2+}] were slower and more prolonged than the fast oscillations of the cytosolic compartment. Additional experiments were carried out in hippocampal slices from adult mice, using a muscarinic agonist (Carbachol, CCH, Figure 5E)

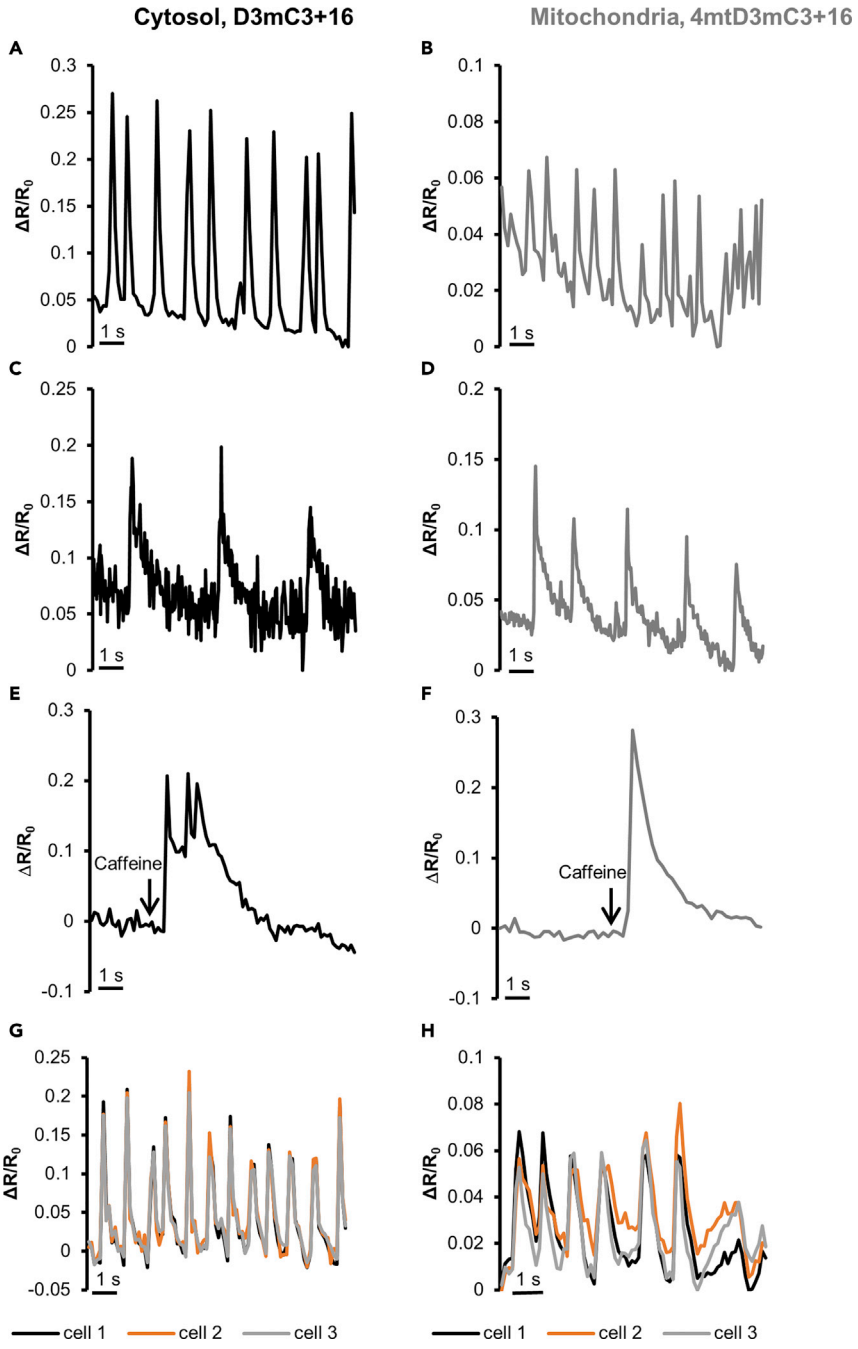

Figure 4. Monitoring [Ca^{2+}] Changes in Cardiomyocytes

Representative traces of spontaneous Ca^{2+} oscillations in neonatal rat cardiomyocytes expressing AAV9-CMV-D3mC3+16 (A) or AAV9-CMV-4mtD3mC3+16 (B). Representative traces of spontaneous Ca^{2+} oscillations in adult cardiomyocytes isolated from mice injected with AAV9-CMV-D3mC3+16 (C) or AAV9-CMV-4mtD3mC3+16 (D). Representative traces of [Ca^{2+}] changes in response to caffeine in adult cardiomyocytes from mice injected with AAV9-CMV-D3mC3+16 (E) or AAV9-CMV-4mtD3mC3+16 (F). Representative traces of spontaneous Ca^{2+} oscillations in human induced pluripotent stem cell-derived cardiomyocytes expressing AAV9-CMV-D3mC3+16 (G) or AAV9-CMV-4mtD3mC3+16 (H). Data are plotted as $\Delta R/R_0$. See also Figure S3.

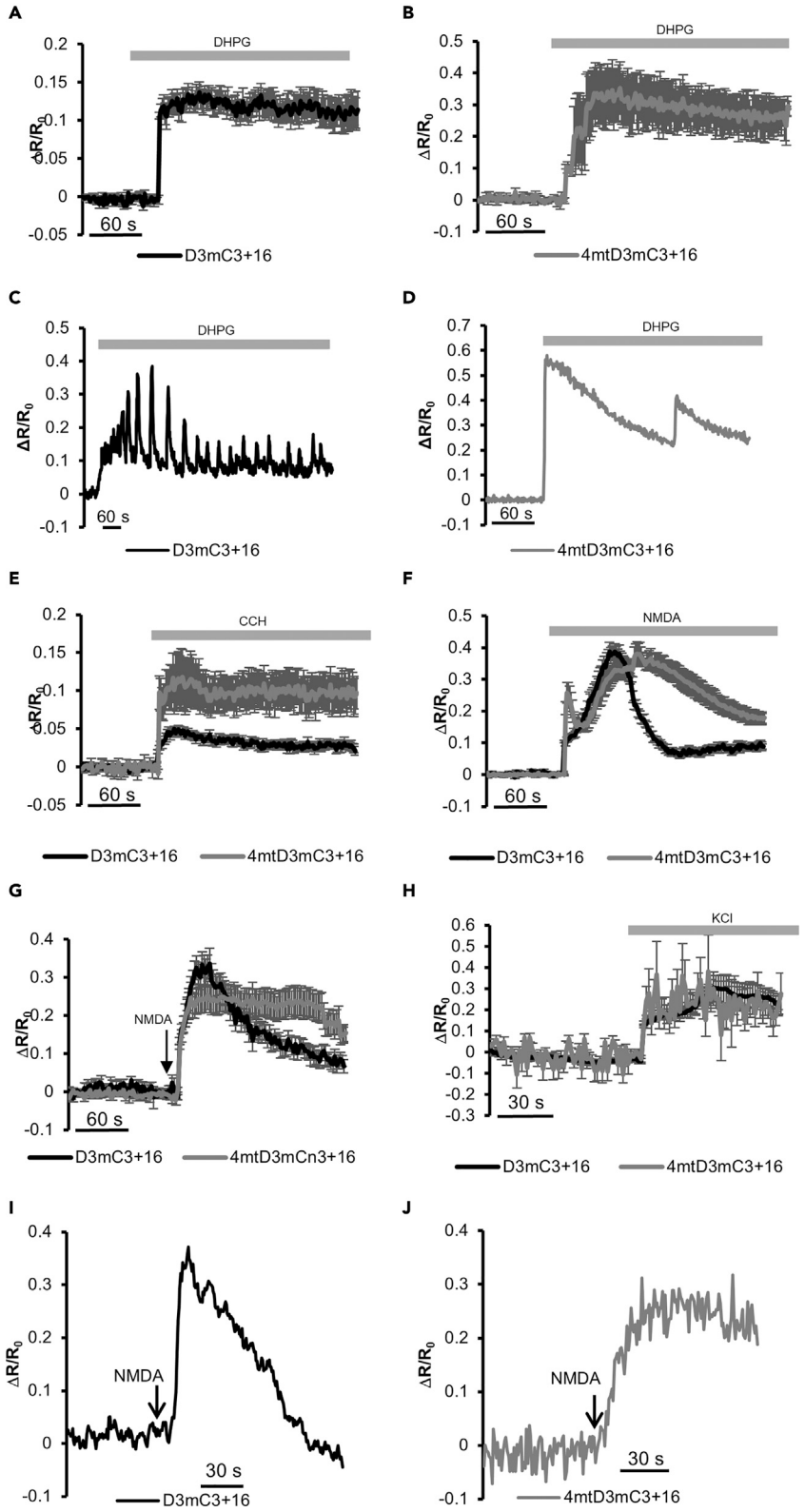
A
DHPG
ΔR/R0
60 s
D3mC3+16
B
DHPG
ΔR/R0
60 s
4mtD3mC3+16
C
DHPG
ΔR/R0
60 s
D3mC3+16
D
DHPG
ΔR/R0
60 s
4mtD3mC3+16
E
CCH
ΔR/R0
60 s
D3mC3+16
4mtD3mC3+16
F
NMDA
ΔR/R0
60 s
D3mC3+16
4mtD3mC3+16
G
NMDA
ΔR/R0
60 s
D3mC3+16
4mtD3mCn3+16
H
KCl
ΔR/R0
30 s
D3mC3+16
4mtD3mC3+16
I
NMDA
ΔR/R0
30 s
D3mC3+16
J
NMDA
ΔR/R0
30 s
4mtD3mC3+16

Figure 5. Monitoring [Ca^{2+}] Changes in the Brain: Hippocampus Slices from Mouse, Somatosensory Cortex Slices from Mouse, and *In Vivo* Mouse Cortex

(A and B) Average traces of Ca^{2+} rise induced by DHPG (50 μM) in neurons of hippocampal slices from mice injected with AAV9-syn-D3mC3+16 (A) or AAV9-syn-4mtD3mC3+16 (B) of N ≥ 4 cells.

(C and D) Representative traces of Ca^{2+} rise induced by DHPG in neurons of hippocampal slices from mice injected with AAV9-syn-D3mC3+16 (C) or AAV9-syn-4mtD3mC3+16 (D).

(E) Average traces of Ca^{2+} rise induced by carbachol (CCH, 500 μM) in neurons of hippocampal slices from mice injected with AAV9-syn-D3mC3+16 (black) or AAV9-syn-4mtD3mC3+16 (gray). N ≥ 5.

(F) Average traces of Ca^{2+} rise induced by perfusion of NMDA 50 μM in neurons of hippocampal slices from mice injected with AAV9-syn-D3mC3+16 (black) or AAV9-syn-4mtD3mC3+16 (gray). N ≥ 10.

(G) Average traces of Ca^{2+} rise induced by neuronal depolarization induced by NMDA receptor activation with 1 mM NMDA (puff administration) in neurons of cortical slices from mice slices from mice injected with AAV9-syn-D3mC3+16 (black) or AAV9-syn-4mtD3mC3+16 (gray). N ≥ 22.

(H) Average traces of Ca^{2+} rise induced by neuronal depolarization with 30 mM KCl in neurons of cortical slices from mice slices from mice infected with AAV9-syn-D3mC3+16 (black) or AAV9-syn-4mtD3mC3+16 (gray). N ≥ 5.

(I and J) *In vivo* experiment showing representative traces of Ca^{2+} rise induced by NMDA receptor activation with 1 mM NMDA (puff administration) in neurons from mice injected with AAV9-syn-D3mC3+16 (I) or AAV9-syn-4mtD3mC3+16 (J).

[Ca^{2+}] changes have been measured in neuronal cell bodies. Data are plotted as $\Delta R/R_0$.

See also Figures S4–S7.

or the ionotropic glutamatergic agonist (N-methyl-D-aspartate, NMDA, Figure 5F), and in somatosensory slices from 2-week old animals upon local application of the glutamatergic agonist NMDA (Figures 5G and S7C–S7F) and depolarization with KCl (Figure 5H). Spontaneous Ca^{2+} oscillations were rarely and randomly observed in the cytosol of neurons of hippocampal slices expressing AAV9-syn-D3mC3+16 (Figure S7G), whereas no spontaneous Ca^{2+} spikes were detected in the mitochondrial compartment.

We finally tested the ability of both probes to detect Ca^{2+} changes *in vivo*. We performed two-photon Ca^{2+} imaging experiments in the cortex of anesthetized mice and locally applied NMDA (1 mM). As expected, we recorded large rise in [Ca^{2+}] in both cytosolic and mitochondrial compartments (Figures 5I and 5J). It is worth noting that, despite the substantial movements due to blood flow and respiration, we were able to record a stable basal mitochondrial Ca^{2+} level, confirming the efficacy of the ratiometric measurement to correct such characteristic confounding artifacts of *in vivo* imaging (Figures 5I and 5J).

DISCUSSION

The central role of Ca^{2+} signaling in the regulation of physiological and pathological processes, as well as the importance of mitochondria in this process, is widely accepted (Rizzuto et al., 2012). Thanks to the development of GECIs, the role of subcellular compartments in Ca^{2+} regulation has been intensively explored; however, their role *in vivo* remains still largely based on indirect information (Pendin et al., 2015). The main reason for this difficulty in monitoring organelle Ca^{2+} handling directly and *in vivo* largely depends on the limitations of the available targeted Ca^{2+} indicators. Movement of the samples (due to breathing, heart- beat, and blood flow) or of the organelle themselves, relatively low fluorescence of ratiometric indicators (ideal for correcting movement artifacts), mislocalization of the expressed probes, pH sensitivity, and photobleaching are particularly relevant problems for investigating mitochondrial Ca^{2+} handling *in vivo*. To overcome these drawbacks, we decided to improve the properties of a widely used FRET-based Ca^{2+} indicator, i.e., the Cameleons, by extensively modifying the primary structure. In particular, we have (1) modified the N-terminus of the 4mtD3cpv, by eliminating a potential additional methionine initiation site (that could be in part responsible for the mistargeting of the original probe to the cytosol) and increasing the number of amphiphilic amino acids in each of the four targeting sequences (i.e., four repeats of the human cytochrome *c* oxidase subunit VIII mitochondria-targeting peptide); (2) substituted ECFP with the more brilliant and less pH sensitive isoform mCerulean3; (3) introduced a flexible linker between the two Ca^{2+} sensor domains (calmodulin and M13). The cytosolic and mitochondrial targeted probes, D3mC3+16 and 4mtD3mC3+16, have been extensively characterized *in situ*, and they show a clear improvement in brightness, photostability, selective localization (for the mitochondrial version), and reduced pH sensitivity. Although most of the improvements were somehow predictable, it is still unclear why the simple substitution of ECFP with another very similar FP isoform results in a drastic modification of R_{max}/R_{min} in response to Ca^{2+}. However, similar examples exist, such as that observed by Thestrup et al. (2014). The strategy of introducing an artificial poly-Gly linker was successful in the mitochondrial target probe and can, in principle, be generalized also to other probes, at least those

that rely on two distinct sensor elements for their functionality. However, the same approach failed in the complete recovery of this drawback in the cytosolic probe. Despite that we do not have a conclusive explanation, we can hypothesize that the different environments between the cytosol and the mitochondria, in terms of pH, temperature (Chrétien et al., 2018), and protein composition, can affect many photophysical properties of both FPs and Ca^{2+}-binding domains.

A debated issue in the mitochondrial field is the amplitude of Ca^{2+} transients that can be experienced by mitochondrial matrix upon stimulation of IP_3R, i.e., up to 3 μM (Kristián et al., 2002; Chalmers and Nicholls, 2003) or up to tenths or hundreds of micromoles (Montero et al., 2000, 2002; Arnaudeau et al., 2001; Pinton et al., 2004). The values reported here, based on an accurate *in situ* calibration of the Cameleons, are much closer to those obtained with mitochondrial low-affinity aequorin than those previously reported with many other GECIs and chemical dyes. The peak $[Ca^{2+}]_m$ here monitored with the Cameleons (that have an affinity for Ca^{2+} much lower than chemical dyes and of most other mitochondrial GECIs) are similar to those measured previously using ratiometric pericams (Filippin et al., 2003) or using a low-affinity Cameleon (Palmer et al., 2006). The average Ca^{2+} peaks reported here, however, are still lower than those measured with mutated aequorin. However, it should be stressed that (1) the average values of the $[Ca^{2+}]$ here reported using 4mtD3mC3 and 4mtD3mC3+16 are substantially underestimated given our choice to selectively eliminate the more strongly responding cells/organelles (see Figures 2F and 2G) and (2) the very high Ca^{2+} values reported by aequorin (averaged over all cells) depend also on the intrinsic characteristics of the aequorin signal calibration that is dominated by the most responsive cells/organelles (for review see Rizzuto and Pozzan, 2006).

Given the recent interest in the FLIM technique to study cellular signaling, we then exploit TCSPC (time-correlated single-photon counting) FLIM-FRET analysis. The use of FLIM microscopy, employing both time and frequency domain approaches, is becoming quite popular not only in classical biophysical studies *in vitro* but also for studying intracellular dynamics in cells, either *in situ* (Klarenbeek et al., 2011; Laine et al., 2012; Zhao et al., 2015) or *in vivo* (Omer et al., 2014; Raspe et al., 2016; Zhao et al., 2015). Here we show that the single exponential lifetime of mCerulean3 allows a precise evaluation of FRET efficiency and increases the dynamic range compared with ECFP-based Cameleon. One unexpected result was the pronounced pH sensitivity of lifetime, in particular in the case of the mitochondrial probe. At low $[Ca^{2+}]$ and at pH 7.0, there is an important and heterogeneous reduction of the acceptor rise term in many cells. This effect is not observed at pH 7.0 in the cytosolic probe or for the mitochondrial sensor in the physiological pH range 7.5–8.0. Although we do not have a clear explanation for this phenomenon, we can hypothesize that it could depend on some specific event occurring in the mitochondrial matrix at this non-physiological pH value. Indeed, changes in the mitochondrial environment have been reported to impact on FPs lifetime (Rieger et al., 2017; Sohnel et al., 2016). However, combining acceptor rise term and lifetime analysis, we revealed an unpredicted consequence of MCU and/or MICU1 overexpression, i.e., a significant acidification of matrix pH at least in a subpopulation of cells (then confirmed by direct measurement with a mitochondria-targeted pH sensitive probe).

After this accurate evaluation of the improved performance of the probes in living cells, we generated AAV9 to express them in primary cultures (neurons and cardiomyocytes), brain slices, and *in vivo* in mouse brain cortex. The data obtained in these models confirm the excellent signal to noise ratio of the mCerulean3-based probes and provide the proof of principle for an *in situ* and *in vivo* evaluation of cytosolic and mitochondrial Ca^{2+} dynamics upon different stimulation protocols, allowing the dissection of different patterns of neurotransmission. In particular, spontaneous synchronized oscillatory activity has been detected in different cardiomyocyte models with both cytosolic and mitochondrial probes. Spontaneous activity has been recorded in both neuronal primary cultures and brain slices; cytosolic and mitochondrial Ca^{2+} changes have been easily monitored in cultured neurons, acute brain slices, and *in vivo* using different pharmacological stimuli.

Generally, the main obstacle preventing the extensive use of Cameleons (and other FRET sensors based on CFP/YFP couple) is the relatively low fluorescence quantum yield of the donor. The substantial increase in the signal to noise ratio we obtained in mCerulean-based sensors could allow experiments in cells with low expression levels that otherwise will be troublesome. In addition, they will also allow quantitative measurements by FLIM, which would be impossible with CFP-based probes because of the double exponential lifetime of this variant, thus expanding the available tools for studying Ca^{2+} signaling *in vivo*.

In conclusion, the mCerulean3-based Cameleons we generated are updated versions of the original probes with a number of improvements in their photo-physical properties that allow their usage in both intensity- and lifetime-based approaches and in different biological contexts. Although the dynamic range of Cameleons in response to [Ca^{2+}] changes is lower compared with the best intensity-based probes, the FRET-based indicators appear superior to correct movement artifacts, photobleaching, and pH sensitivity, and most relevant, they allow one to quantitatively estimate the values of [Ca^{2+}] at rest and during stimulation.

Limitations of the Study

Beyond the reported advantages, mCeruelean3-based Cameleon probes retain some of the general limitations of FRET-based biosensors, i.e., lower dynamic range and lower fluorescence intensity compared with chemical indicators or to some of the single FP-based sensors. Furthermore, although pH sensitivity has been ameliorated, pH can still affect some properties of mCerulean3-based Cameleons. Lifetime measurements, and in particular the rise term analysis of 4mtD3mCerulean3+16, can help in distinguishing Ca^{2+} and pH effects on the FRET signal. Finally, since Cameleons are high-molecular-weight sensors, their fusion with other cDNAs in viral vector with small expression cassettes is hampered.

METHODS

All methods can be found in the accompanying Transparent Methods supplemental file.

SUPPLEMENTAL INFORMATION

Supplemental Information can be found online at https://doi.org/10.1016/j.isci.2019.05.031.

ACKNOWLEDGMENTS

We acknowledge M.A. Rizzo (University of Maryland School of Medicine) for mCerulean3 cDNA, N. Demaurex (University of Geneva) for mt-SyPher cDNA, D. De Stefani (University of Padua) for mtGCaMP6f cDNA, and K. Deisseroth (Stanford University School of Medicine) for pAAV-Syn-ChR2(H134R)-GFP cDNA.

The work described in this article was supported by grants from Fondazione Cassa di Risparmio di Padua e Rovigo (CARIPARO Foundation), Veneto Region (Rete di infrastrutture e supporto dell'innovazione biotecnologica [RISIB Project]), Consiglio Nazionale delle Ricerche (CNR) Special Project Aging, Italian Ministry of University and Research (Fondo per gli Investimenti della Ricerca di Base [FIRB Project] and Euro Bioimaging Project), Telethon Italy Grant GGP16029A and Progetti di Rilevante Interesse Nazionale (PRIN) to T.P., the Italian Ministry of University and Research (Fondo per gli Investimenti della Ricerca di Base [FIRB Project]) to R.B, Fondazione Cassa di Risparmio di Padua e Rovigo (CARIPARO Foundation) Starting Grant 2015 to D.P., EFSD/Sanofi research grant to N.K., Telethon Italy Grant GGP12265, Fondazione Cassa di Risparmio di Padua e Rovigo (CARIPARO Foundation), Consiglio Nazionale delle Ricerche (CNR) Special Project Aging, Fondo per gli Investimenti della Ricerca di Base Grant RBAP11X42L to G.C., and UNIPD funds for research equipment 2015.

AUTHOR CONTRIBUTIONS

Conceptualization: T.P. and R.B.; Methodology: L.Z., M.G., T.P., and C.F.; Formal Analysis: E.G., D.P., and I.F.; Investigation: E.G., D.P., I.F., A.L., L.G., M.G.-G., M.S., L.M., and N.K.; Resources: T.P., G.C., D.P., N.K., and R.B.; Writing – Original Draft: E.G.; Writing – Review & Editing: D.P., I.F., C.F., G.C., R.B., and T.P.; Visualization: E.G. and I.F.; Project Administration: T.P. and R.B.; Funding Acquisition: T.P., R.B., D.P., N.K., and G.C.

DECLARATION OF INTERESTS

The authors declare no competing interests.

Received: March 1, 2019
Revised: April 26, 2019
Accepted: May 22, 2019
Published: June 28, 2019

REFERENCES

Arnaudeau, S., Kelley, W.L., Walsh, J.V., Jr., and Demaurex, N. (2001). Mitochondria recycle Ca^{2+} to the endoplasmic reticulum and prevent the depletion of neighboring endoplasmic reticulum regions. J. Biol. Chem. *276*, 29430–29439.

Bish, L.T., Morine, K., Sleeper, M.M., Sanmiguel, J., Wu, D., Gao, G.P., Wilson, J.M., and Sweeney, H.L. (2008). Adeno-associated virus (AAV) serotype 9 provides global cardiac gene transfer superior to AAV1, AAV6, AAV7, and AAV8 in the mouse and rat. Hum. Gene Ther. *19*, 1359–1368.

Borst, J.W., Laptenok, S.P., Westphal, A.H., Kuhnemuth, R., Hornen, H., Visser, N.V., Kalinin, S., Aker, J., van Hoek, A., Seidel, C.A., et al. (2008). Structural changes of yellow Cameleon domains observed by quantitative FRET analysis and polarized fluorescence correlation spectroscopy. Biophys. J. *95*, 5399–5411.

Cárdenas, C., Miller, R.A., Smith, I., Bui, T., Molgó, J., Müller, M., Vais, H., Cheung, K.H., Yang, J., Parker, I., et al. (2010). Essential regulation of cell bioenergetics by constitutive InsP3 receptor Ca2+ transfer to mitochondria. Cell *142*, 270–283.

Chalmers, S., and Nicholls, D.G. (2003). The relationship between free and total calcium concentrations in the matrix of liver and brain mitochondria. J. Biol. Chem. *278*, 19062–19070.

Chichili, V.P.R., Kumar, V., and Sivaraman, J. (2013). Linkers in the structural biology of protein-protein interactions. Protein Sci. *22*, 153–167.

Chrétien, D., Bénit, P., Ha, H.H., Keipert, S., El-Khoury, R., Chang, Y.T., Jastroch, M., Jacobs, H.T., Rustin, P., and Rak, M. (2018). Mitochondria are physiologically maintained at close to 50°C. PLoS Biol. *16*, e2003992.

Csordas, G., Golenar, T., Seifert, E.L., Kamer, K.J., Sancak, Y., Perocchi, F., Moffat, C., Weaver, D., de la Fuente Perez, S., Bogorad, R., et al. (2013). MICU1 controls both the threshold and cooperative activation of the mitochondrial Ca^{+} uniporter. Cell Metab. *17*, 976–987.

Filippin, L., Magalhaes, P.J., Di Benedetto, G., Colella, M., and Pozzan, T. (2003). Stable interactions between mitochondria and endoplasmic reticulum allow rapid accumulation of calcium in a subpopulation of mitochondria. J. Biol. Chem. *278*, 39224–39234.

Filippin, L., Abad, M.C., Gastaldello, S., Magalhaes, P.J., Sandona, D., and Pozzan, T. (2005). Improved strategies for the delivery of GFP-based Ca2+ sensors into the mitochondrial matrix. Cell Calcium *37*, 129–136.

Foust, K.D., Nurre, E., Montgomery, C.L., Hernandez, A., Chan, C.M., and Kaspar, B.K. (2009). Intravascular AAV9 preferentially targets neonatal neurons and adult astrocytes. Nat. Biotechnol. *27*, 59–65.

Geiger, A., Russo, L., Gensch, T., Thestrup, T., Becker, S., Hopfner, K.P., Griesinger, C., Witte, G., and Griesbeck, O. (2012). Correlating calcium binding, forster resonance energy transfer, and conformational change in the biosensor TN-XXL. Biophys. J. *102*, 2401–2410.

Goedhart, J., van Weeren, L., Hink, M.A., Vischer, N.O., Jalink, K., and Gadella, T.W., Jr. (2010). Bright cyan fluorescent protein variants identified by fluorescence lifetime screening. Nat. Methods *7*, 137–139.

Hofer, A.M., Fasolato, C., and Pozzan, T. (1998). Capacitative Ca2+ entry is closely linked to the filling state of internal Ca2+ stores: a study using simultaneous measurements of ICRAC and intraluminal [Ca2+]. J. Cell Biol. *140*, 325–334.

Horikawa, K., Yamada, Y., Matsuda, T., Kobayashi, K., Hashimoto, M., Matsu-ura, T., Miyawaki, A., Michikawa, T., Mikoshiba, K., and Nagai, T. (2010). Spontaneous network activity visualized by ultrasensitive Ca2+ indicators, yellow Cameleon-Nano. Nat. Methods *7*, 729–U788.

Klarenbeek, J.B., Goedhart, J., Hink, M.A., Gadella, T.W.J., and Jalink, K. (2011). A mTurquoise-based cAMP sensor for both FLIM and ratiometric read-out has improved dynamic range. PLoS One *6*, e19170.

Koldenkova, V.P., and Nagai, T. (2013). Genetically encoded Ca2+ indicators: properties and evaluation. Biochim. Biophys. Acta *1833*, 1787–1797.

Kristián, T., Weatherby, T.M., Bates, T.E., and Fiskum, G. (2002). Heterogeneity of the calcium-induced permeability transition in isolated non-synaptic brain mitochondria. J. Neurochem. *83*, 1297–1308.

Kugler, S., Meyn, L., Holzmuller, H., Gerhardt, E., Isenmann, S., Schulz, J.B., and Bahr, M. (2001). Neuron-specific expression of therapeutic proteins: evaluation of different cellular promoters in recombinant adenoviral vectors. Mol. Cell. Neurosci. *17*, 78–96.

Laine, R., Stuckey, D.W., Manning, H., Warren, S.C., Kennedy, G., Carling, D., Dunsby, C., Sardini, A., and French, P.M.W. (2012). Fluorescence lifetime readouts of troponin-C-based calcium FRET sensors: a quantitative comparison of CFP and mTFP1 as donor fluorophores. PLoS One *7*, 1–16.

Mallilankaraman, K., Doonan, P., Cardenas, C., Chandramoorthy, H.C., Muller, M., Miller, R., Hoffman, N.E., Gandhirajan, R.K., Molgo, J., Birnbaum, M.J., et al. (2012). MICU1 is an essential gatekeeper for MCU-mediated mitochondrial Ca(2+) uptake that regulates cell survival. Cell *151*, 630–644.

Mammucari, C., Gherardi, G., Zamparo, I., Raffaello, A., Boncompagni, S., Chemello, F., Cagnin, S., Braga, A., Zanin, S., Pallafacchina, G., et al. (2015). The mitochondrial calcium uniporter controls skeletal muscle trophism *in vivo*. Cell Rep. *10*, 1269–1279.

Marcu, L., French, P., and Elson, D.S. (2014). Fluorescence Lifetime Spectroscopy and Imaging Principles and Applications in Biomedical Diagnostic (CRC Press).

Markwardt, M.L., Kremers, G.J., Kraft, C.A., Ray, K., Cranfill, P.J.C., Wilson, K.A., Day, R.N., Wachter, R.M., Davidson, M.W., and Rizzo, M.A. (2011). An improved cerulean fluorescent protein with enhanced brightness and reduced reversible photoswitching. PLoS One *6*, e17896.

Millington, M., Grindlay, G.J., Altenbach, K., Neely, R.K., Kolch, W., Bencina, M., Read, N.D., Jones, A.C., Dryden, D.T.F., and Magennis, S.W. (2007). High-precision FLIM-FRET in fixed and living cells reveals heterogeneity in a simple CFP-YFP fusion protein. Biophys. Chem. *127*, 155–164.

Montero, M., Alonso, M.T., Carnicero, E., Cuchillo-Ibáñez, I., Albillos, A., García, A.G., García-Sancho, J., and Alvarez, J. (2000). Chromaffin-cell stimulation triggers fast millimolar mitochondrial Ca2+ transients that modulate secretion. Nat. Cell Biol. *2*, 57–61.

Montero, M., Lobatón, C.D., Moreno, A., and Alvarez, J. (2002). A novel regulatory mechanism of the mitochondrial Ca2+ uniporter revealed by the p38 mitogen-activated protein kinase inhibitor SB202190. FASEB J. *16*, 1955–1957.

Nagai, T., Yamada, S., Tominaga, T., Ichikawa, M., and Miyawaki, A. (2004). Expanded dynamic range of fluorescent indicators for Ca2+ by circularly permuted yellow fluorescent proteins. Proc. Natl. Acad. Sci. U S A *101*, 10554–10559.

Omer, T., Zhao, L.L., Intes, X., and Hahn, J. (2014). Reduced temporal sampling effect on accuracy of time-domain fluorescence lifetime Forster resonance energy transfer. J. Biomed. Opt. *19*, 086023.

Ostergaard, G., Hansen, H.N., and Ottesen, J.L. (2010). Physiological, hematological, and clinical chemistry parameters, including conversion factors. In Handbook of Laboratory Animal Science, Volume I: Essential Principles and Practices, Third Edition, *Vol. 1*, J. Hau and S.J. Schapiro, eds. (CRC Press), pp. 667–707.

Pacak, C.A., Mah, C.S., Thattaliyath, B.D., Conlon, T.J., Lewis, M.A., Cloutier, D.E., Zolotukhin, I., Tarantal, A.F., and Byrne, B.J. (2006). Recombinant adeno-associated virus serotype 9 leads to preferential cardiac transduction *in vivo*. Circ. Res. *99*, E3–E9.

Palmer, A.E., and Tsien, R.Y. (2006). Measuring calcium signaling using genetically targetable fluorescent indicators. Nat. Protoc. *1*, 1057–1065.

Palmer, A.E., Giacomello, M., Kortemme, T., Hires, S.A., Lev-Ram, V., Baker, D., and Tsien, R.Y. (2006). Ca2+ indicators based on computationally redesigned calmodulin-peptide pairs. Chem. Biol. *13*, 521–530.

Patron, M., Checchetto, V., Raffaello, A., Teardo, E., Vecellio Reane, D., Mantoan, M., Granatiero, V., Szabo, I., De Stefani, D., and Rizzuto, R. (2014). MICU1 and MICU2 finely tune the Mitochondrial Ca2+ uniporter by exerting opposite effects on MCU activity. Mol. Cell *53*, 726–737.

Pendin, D., Greotti, E., Filadi, R., and Pozzan, T. (2015). Spying on organelle Ca2+ in living cells:the mitochondrial point of view. J. Endocrinol. Invest. *38*, 39–45.

Pendin, D., Greotti, E., Lefkimmiatis, K., and Pozzan, T. (2017). Exploring cells with targeted biosensors. J. Gen. Physiol. *149*, 1–36.

Pinton, P., Leo, S., Wieckowski, M.R., Di Benedetto, G., and Rizzuto, R. (2004). Long-term modulation of mitochondrial Ca2+ signals by

protein kinase C isozymes. J. Cell Biol. *165*, 223–232.

Poburko, D., and Demaurex, N. (2012). Regulation of the mitochondrial proton gradient by cytosolic Ca2+ signals. Pflug Arch. Eur. J. Phys. *464*, 19–26.

Raspe, M., Kedziora, K.M., van den Broek, B., Zhao, Q., de Jong, S., Herz, J., Mastop, M., Goedhart, J., Gadella, T.W.J., Young, I.T., et al. (2016). siFLIM: single-image frequency-domain FLIM provides fast and photon-efficient lifetime data. Nat. Methods *13*, 501–504.

Rieger, B., Shalaeva, D.N., Sohnel, A.C., Kohl, W., Duwe, P., Mulkidjanian, A.Y., and Busch, K.B. (2017). Lifetime imaging of GFP at CoxVIIIa reports respiratory supercomplex assembly in live ells. Sci. Rep. *7*, 46055.

Rizzuto, R., and Pozzan, T. (2006). Microdomains of intracellular Ca2+: molecular determinants and functional consequences. Physiol. Rev. *86*, 369–408.

Rizzuto, R., De Stefani, D., Raffaello, A., and Mammucari, C. (2012). Mitochondria as sensors and regulators of calcium signalling. Nat. Rev. Mol. Cell Biol. *13*, 566–578.

Sohnel, A.C., Kohl, W., Gregor, I., Enderlein, J., Rieger, B., and Busch, K.B. (2016). Probing of protein localization and shuttling in mitochondrial microcompartments by FLIM with sub-diffraction resolution. Biochim. Biophys. Acta *1857*, 1290–1299.

Thestrup, T., Litzlbauer, J., Bartholomaus, I., Mues, M., Russo, L., Dana, H., Kovalchuk, Y., Liang, Y.J., Kalamakis, G., Laukat, Y., et al. (2014). Optimized ratiometric calcium sensors for functional *in vivo* imaging of neurons and T lymphocytes. Nat. Methods *11*, 175–182.

Tosatto, A., Sommaggio, R., Kummerow, C., Bentham, R.B., Blacker, T.S., Berecz, T., Duchen, M.R., Rosato, A., Bogeski, I., Szabadkai, G., et al. (2016). The mitochondrial calcium uniporter regulates breast cancer progression via HIF-1α. EMBO Mol. Med. *8*, 569–585.

Villoing, A., Ridhoir, M., Cinquin, B., Erard, M., Alvarez, L., Vallverdu, G., Pernot, P., Grailhe, R., Merola, F., and Pasquier, H. (2008). Complex fluorescence of the cyan fluorescent protein: comparisons with the H148D variant and consequences for quantitative cell imaging. Biochemistry *47*, 12483–12492.

Zhao, M., Wan, X.Y., Li, Y., Zhou, W.B., and Peng, L.L. (2015). Multiplexed 3D FRET imaging in deep tissue of live embryos. Sci. Rep. *5*, 13991.

ISCI, Volume *16*

Supplemental Information

mCerulean3-Based Cameleon Sensor to Explore Mitochondrial Ca^{2+} Dynamics *In Vivo*

Elisa Greotti, Ilaria Fortunati, Diana Pendin, Camilla Ferrante, Luisa Galla, Lorena Zentilin, Mauro Giacca, Nina Kaludercic, Moises Di Sante, Letizia Mariotti, Annamaria Lia, Marta Gómez-Gonzalo, Michele Sessolo, Giorgio Carmignoto, Renato Bozio, and Tullio Pozzan

Supplemental Figures

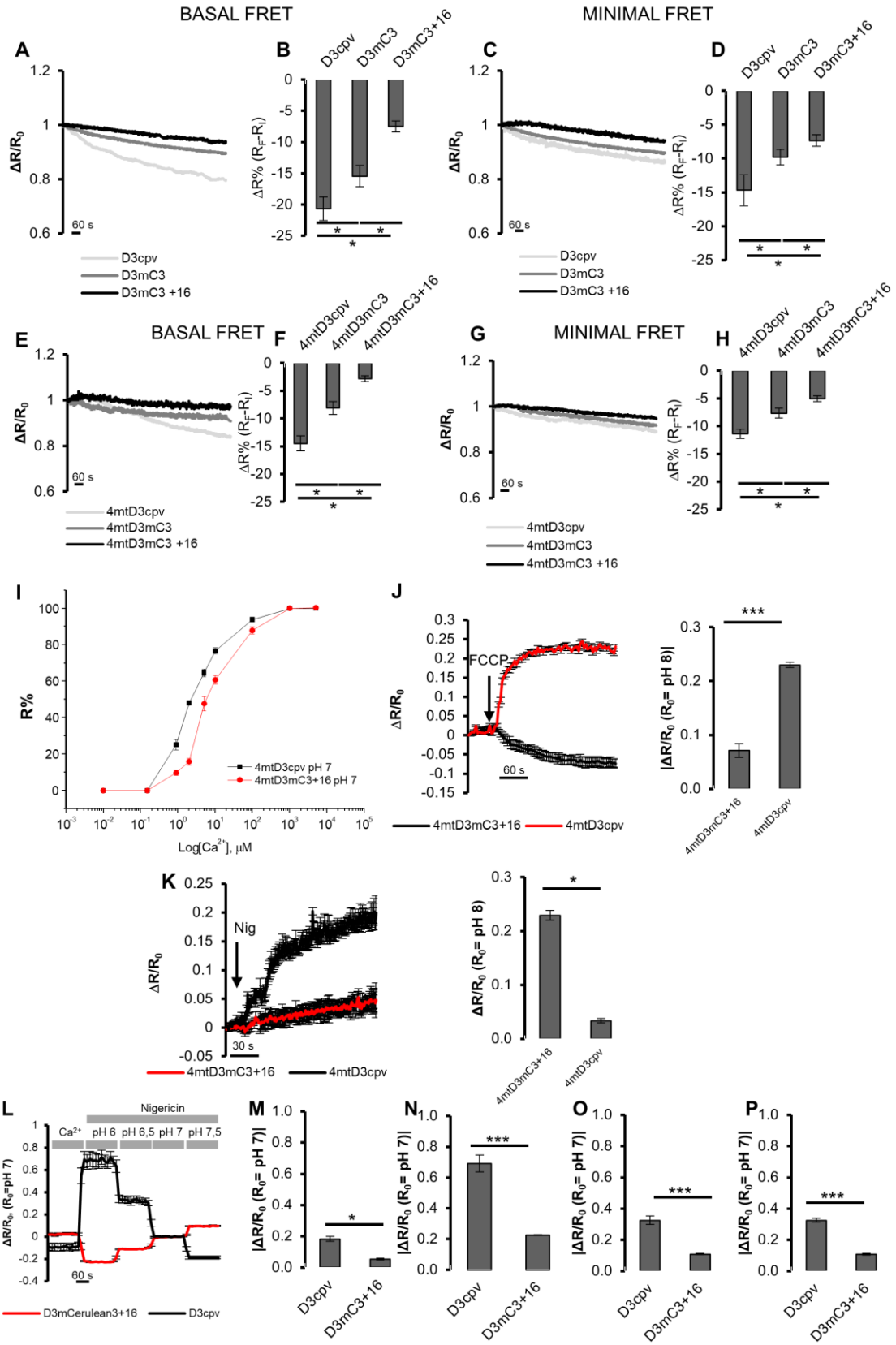

Figure S1. Related to Figure 1. *Improvement in photostability.* **(A-H)** The graphs show the ratio decrease measured by illuminating the sample each second for 20 min in HeLa cells expressing D3cpv (light grey), D3mC3 (grey) and D3mC3+16 (black) in basal FRET condition, *i.e.*, cells bathed in extracellular-like medium containing 1 mM $CaCl_2$ [**A,** representative trace of R changes over time normalized to the initial R (R_0); **B,** mean±SEM of $\Delta R\%(R_i-R_f)$, where $\Delta R\%$ is calculated as % of the reduction in R between its initial value (R_i) and its value after 20 minutes (R_f)] and minimal FRET condition, *i.e.*, cells bathed in extracellular-like medium containing BAPTA 5 µM [**C,** representative trace of R changes over time; **D,** mean±SEM of $\Delta R\%(R_i-R_f)$]; or in HeLa expressing 4mtD3cpv (light grey), 4mtD3mC3 (grey) and 4mtD3mC3+16 (black) in basal FRET condition, *i.e.*, cells bathed in extracellular-like medium containing 1 mM $CaCl_2$ [**E,** representative trace of R changes over time**; F** mean±SEM of $\Delta R\%(R_i-R_f)$] and minimal FRET condition *i.e.* pre-permeabilized cells bathed in intracellular-like medium containing 0.6 mM EGTA and 10 µM FCCP [**G,** representative trace of R changes over time**; H** mean±SEM of $\Delta R\%(R_i-R_f)$]. Data are from N≥15 cells for each condition. **(I-P)** *pH dependency of cytosolic and mitochondrial Cameleon probes.* **(I)** *In situ* Ca^{2+} titration 4mtD3cpv (black trace) or 4mtD3mC3+16 (red trace), along with corresponding fits of the data as mean±SEM of N≥3 cells for each $[Ca^{2+}]$ at pH 7. **(J-P)** Representative traces of pH-sensitivity experiments. **(J**) Effect of acidification from pH 8.0 to 7.0 on R values in mitochondria-targeted probes. *Left.* Representative kinetics of the $\Delta R/R_0$ (where R_0 is the R at physiological pH 8.0) of HeLa cells expressing 4mtD3mC3+16 (black) or 4mtD3cpv (red). All the experiments were carried out in extracellular saline in the presence of 1 mM $CaCl_2$. Where indicated, extracellular-like medium with 5 µM FCCP was added to decrease the mitochondrial matrix pH from 8.0 to 7.0. *Right.* The bar chart shows the absolute value of $\Delta R/R_0$ (where R_0 is the R in physiological condition, *i.e.* pH 8.0) measured in HeLa cells expressing 4mtD3cpv or 4mtD3mC3+16 at pH 7.0 as mean±SEM of N≥21 cells for each condition. Cells expressing 4mtD3cpv displayed a substantial apparent rise of $[Ca^{2+}]$ in the mitochondria upon acidification of matrix pH, while mCerulean3-based Cameleon displayed a small decrease in the R values. Of note, in the original Cameleon the increase in R induced by the pH drop is significantly larger compared to decrease of R in 4mtD3mC3+16. Of note, FCCP treatment, dissipating mitochondrial membrane potential, can reduce not only the pH but also the $[Ca^{2+}]$ in the mitochondrial matrix. **(K)** *Left.* Average traces of the $\Delta R/R_0$ (where R_0 is the R at physiological pH 8.0) of HeLa cells expressing 4mtD3mC3+16 (red) or 4mtD3cpv (black). All the experiments were carried out in K^+-based medium in the absence of external Ca^{2+}. Where indicated, 100 nM Nigericin

was added in order to equilibrate the mitochondrial matrix pH with that of the cytosol (pH from 8.0 to 7.0), without reducing mitochondrial membrane potential and thus mitochondrial matrix [Ca^{2+}]. *Right.* The bar chart shows the value of $\Delta R/R_0$ (where R_0 is the R in physiological condition, *i.e.* pH 8.0) measured in HeLa cells expressing 4mtD3cpv or 4mtD3mC3+16 at pH 7.0 as mean±SEM of N≥53 cells for each condition. With both probes acidification resulted in a rise of R, but the effect is significantly larger in the original Cameleon compared to that observed in cells expressing 4mtD3mC3+16. **(L)** Effect of pH on the R values in cytosolic probes at basal [Ca^{2+}]. Average traces of the $\Delta R/R_0$ (where R_0 is the R at physiological pH 7.0) of HeLa cells expressing D3mC3+16 (red) or D3cpv (black). All the experiments were carried out in the presence of 1 mM $CaCl_2$ and 5 µM nigericin was added to allow pH equilibration. Where indicated the K-based extracellular-like medium at pH 7.4 was substituted with intracellular-like medium at pH 6.0, 6.5, 7.0 and 7.5. **(M-P)** The bar chart shows the absolute value of $\Delta R/R_0$ (where R_0 is the R at physiological pH 7) measured in HeLa cells expressing D3cpv or D3mC3+16 at pH 7.0 **(M)**, 6.0 **(N)**, 6.5 **(O)**, 7.5 **(P)** as mean±SEM of N≥23 cells for each condition. R is significantly increased by pH acidification in cells expressing D3cpv, but only slightly reduced by acidification and increased by alkalinization with D3mC3+16, confirming the lower sensitivity to pH changes of the probes generated. * $p<0.05$, ANOVA and Bonferroni post hoc. * $p<0.05$; ** $p<0.01$; *** $p<0.0001$ with Wilcoxon analysis.

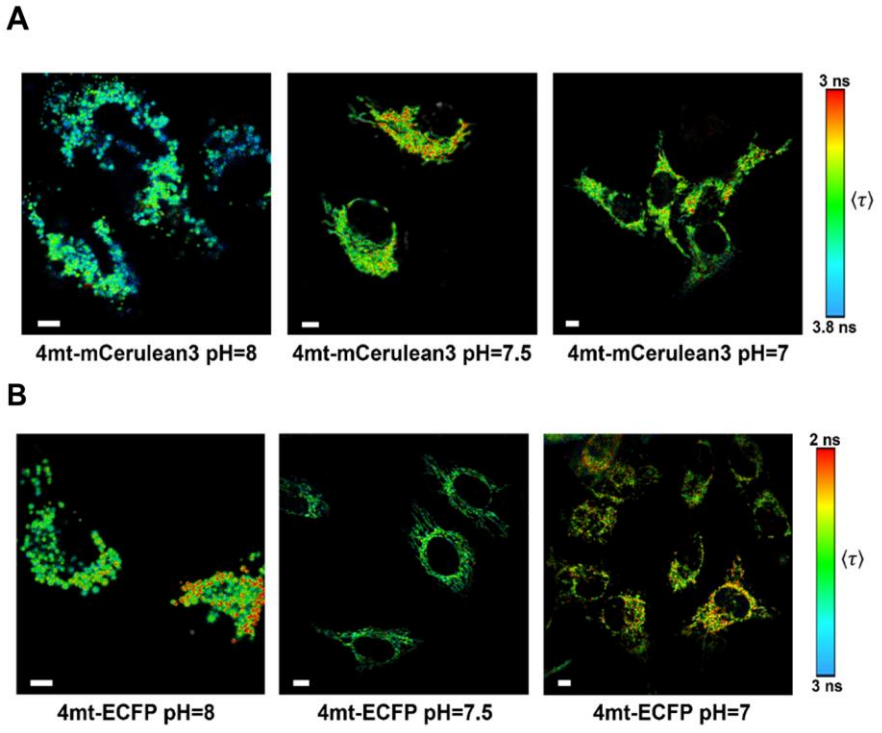
A
3 ns
⟨τ⟩
3.8 ns
4mt-mCerulean3 pH=8
4mt-mCerulean3 pH=7.5
4mt-mCerulean3 pH=7
B
2 ns
⟨τ⟩
3 ns
4mt-ECFP pH=8
4mt-ECFP pH=7.5
4mt-ECFP pH=7

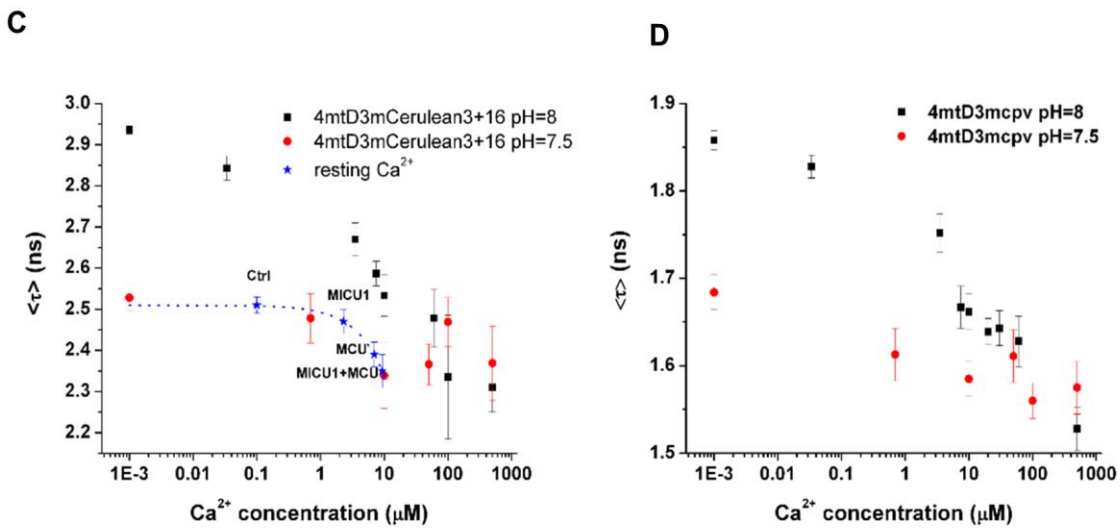
C
4mtD3mCerulean3+16 pH=8
4mtD3mCerulean3+16 pH=7.5
resting Ca2+
Ctrl
MICU1
MCU
MICU1+MCU1
<τ> (ns)
Ca2+ concentration (μM)
D
4mtD3mcpv pH=8
4mtD3mcpv pH=7.5
<τ> (ns)
Ca2+ concentration (μM)

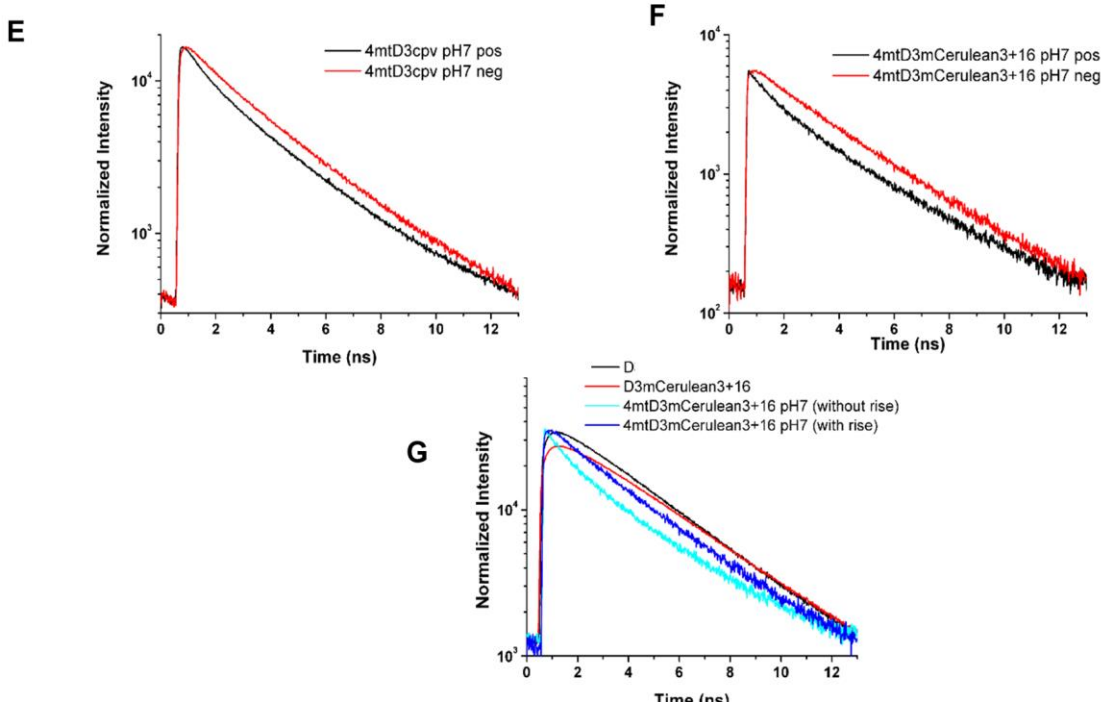
E
4mtD3cpv pH7 pos
4mtD3cpv pH7 neg
Normalized Intensity
Time (ns)
F
4mtD3mCerulean3+16 pH7 pos
4mtD3mCerulean3+16 pH7 neg
Normalized Intensity
Time (ns)
G
D
D3mCerulean3+16
4mtD3mCerulean3+16 pH7 (without rise)
4mtD3mCerulean3+16 pH7 (with rise)
Normalized Intensity
Time (ns)

Figure S2. Related to Figure 3. *Fluorescence lifetime analysis in Hela cells.* pH-effect on donor lifetime. HeLa cells expressing only the donors 4mt-mCerulean3 **(A)** or 4mt-ECFP **(B)** were permeabilized with digitonin (without substrates and Ca^{2+} and in presence of the uncoupler FCCP, to equilibrate matrix pH with that of the medium) in intracellular-like medium at pH 8.0, 7.5 and 7.0. **(A**) FLIM images of 4mt-mCerulean3 in intact HeLa cells in resting conditions. FLIM images report the amplitude-weighted lifetime in the 3-3.8 ns range. Scale bar, 10 µm. **(B)** FLIM images of 4mt-ECFP in intact HeLa cells in resting conditions. FLIM images report the amplitude-weighted lifetime in the 2-3 ns range. Both mitochondria-targeted donors display shorter average lifetimes upon pH acidification (donor average lifetimes -*see* the equation for amplitude-weighted lifetime in Transparent Methods- and relative amplitude summarized in **Table S1. Related to Figure 3**). Scale bar, 10 µm. Calibration curves of 4mtD3mCerulea3+16 (**C**) and 4mtD3cpv (**D**) with increasing Ca^{2+} concentrations at pH 8.0 and pH 7.5. y-axis shows the amplitude-weighted lifetimes (τ_{amp}). In **(C)** blue stars refer to τ_{amp} measured with MCU, MICU1 or both MCU and MICU1 overexpressing cells. Acidification causes a reduction in the dynamic range of either probes. Noteworthy, the average donor lifetime at pH 7.0 and 7.5 was shorter than that measured at pH 8.0 at the same [Ca^{2+}] (see **Table S2,4**. **Related to Figure 3** for 4mtD3mC3+16 and **Table S3,5. Related to Figure 3** for 4mtD3cpv). **(E-F)** Normalized fluorescence decay of acceptor moiety in 4mtD3cpv **(E)** or in 4mtD3mC3+16 **(F)** at pH 7.0 in the absence of rise (black) or in the presence of rise (red). **(G)** Normalized fluorescence decay of acceptor moiety in 4mtD3mC3+16 at pH 7.0 in the absence of rise (cyan) or in the presence of rise (blue) and of D3mC3+16 (red) or D3cpv (black). Of note, unlike the mitochondrial sensor, a rise term in the acceptor emission channel is present in all cells at pH 7, which is the physiological cytosolic pH in resting condition (Rink et al., 1982). .

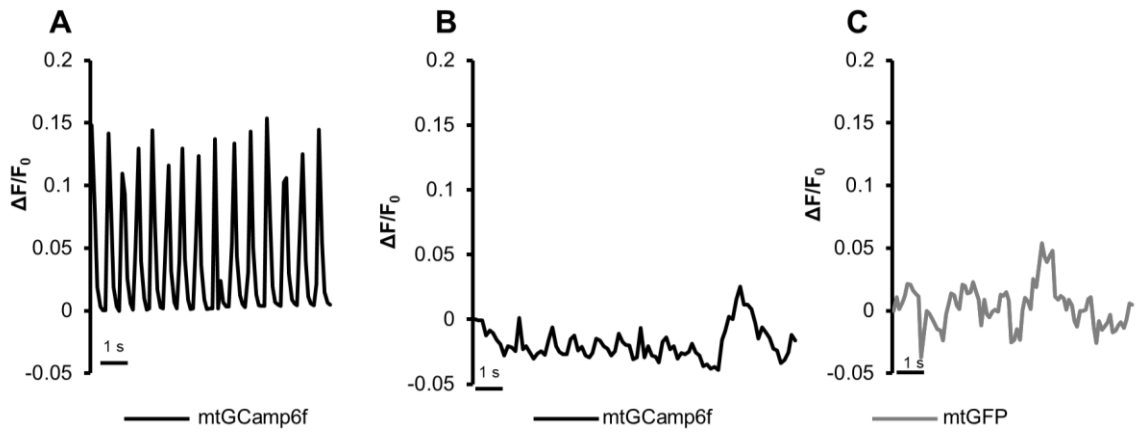

Figure S3. Related to Figure 4. *Monitoring [Ca^{2+}] changes in cardiomyocytes with non-ratiometric sensors*. Representative traces of spontaneous Ca^{2+} oscillations in neonatal rat cardiomyocytes expressing mtGCaMP6f **(A-B)** or mt-GFP**(C)**. Data are presented as $\Delta F/F_0$, where F_0 is the minimal fluorescence recorded.

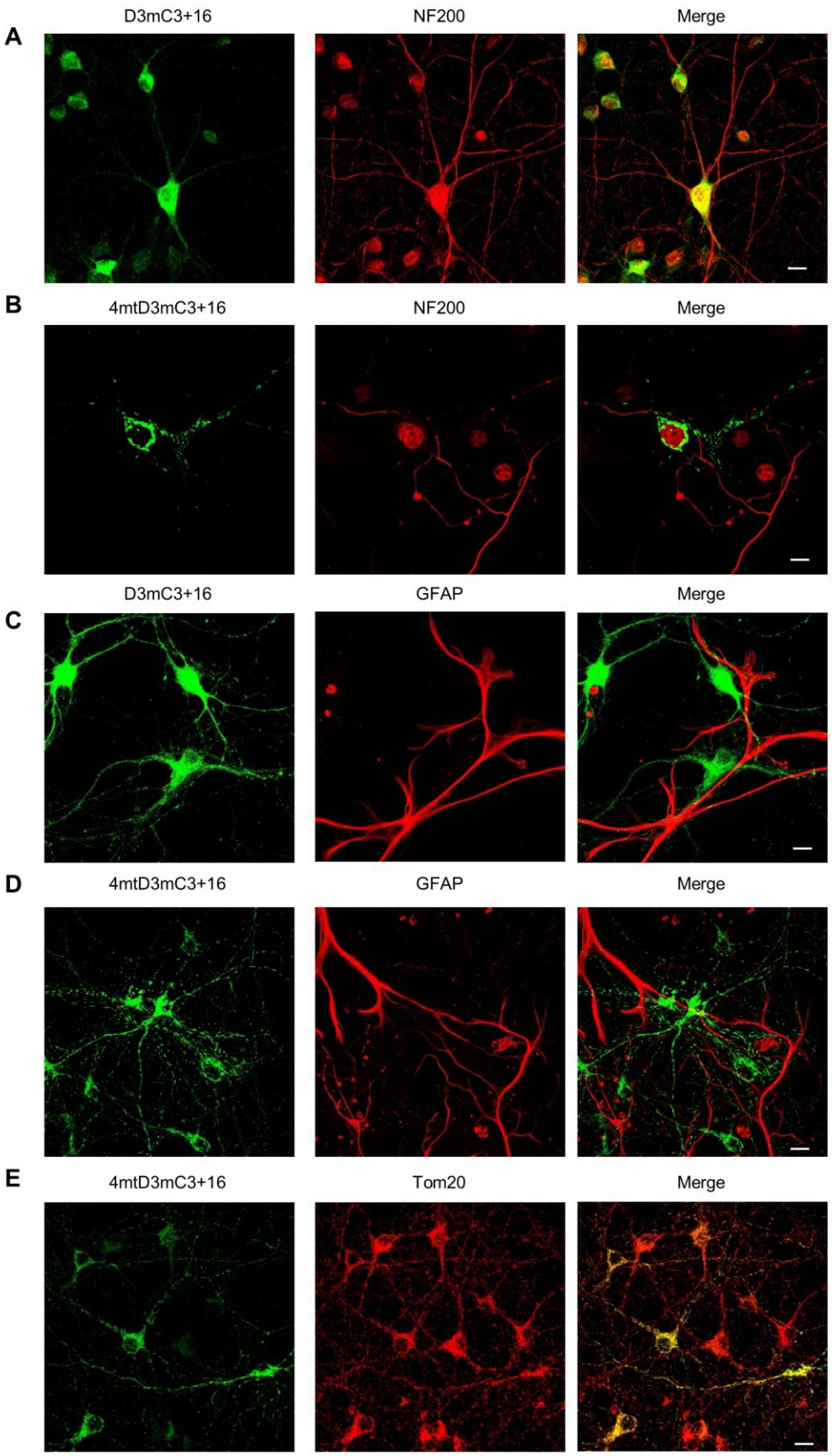
A
D3mC3+16
NF200
Merge
B
4mtD3mC3+16
NF200
Merge
C
D3mC3+16
GFAP
Merge
D
4mtD3mC3+16
GFAP
Merge
E
4mtD3mC3+16
Tom20
Merge

Figure S4. Related to Figure 5. *Proper localization of the mitochondrial and cytosolic probes in cultured neurons*. The cytosolic and mitochondrial localization of the probes in cortical neurons from newborn mice were assessed by immunohistochemistry after 96 hours from infection with AAV9-syn-D3mC3+16 (**A-C**) and AAV9-syn-4mtD3mC3+16 (**B-D-E**). Yellow color indicates co-localization of the D3mC3+16 (**A**) or 4mtD3mC3+16 (**B**) and neurons, labeled with anti-NF200 antibody. The absence of co-localization between D3mC3+16 (**C**) or 4mtD3mC3+16 (**D**) and non-neuronal cells such as astrocytes, labeled with anti-GFAP antibody is shown. The mitochondrial localization of the probe was evaluated by co-localization with a mitochondrial marker, TOM20 (**E**). Yellow color indicates co-localization with mitochondria and 4mtD3mC3+16. Scale bar, 10 µm.

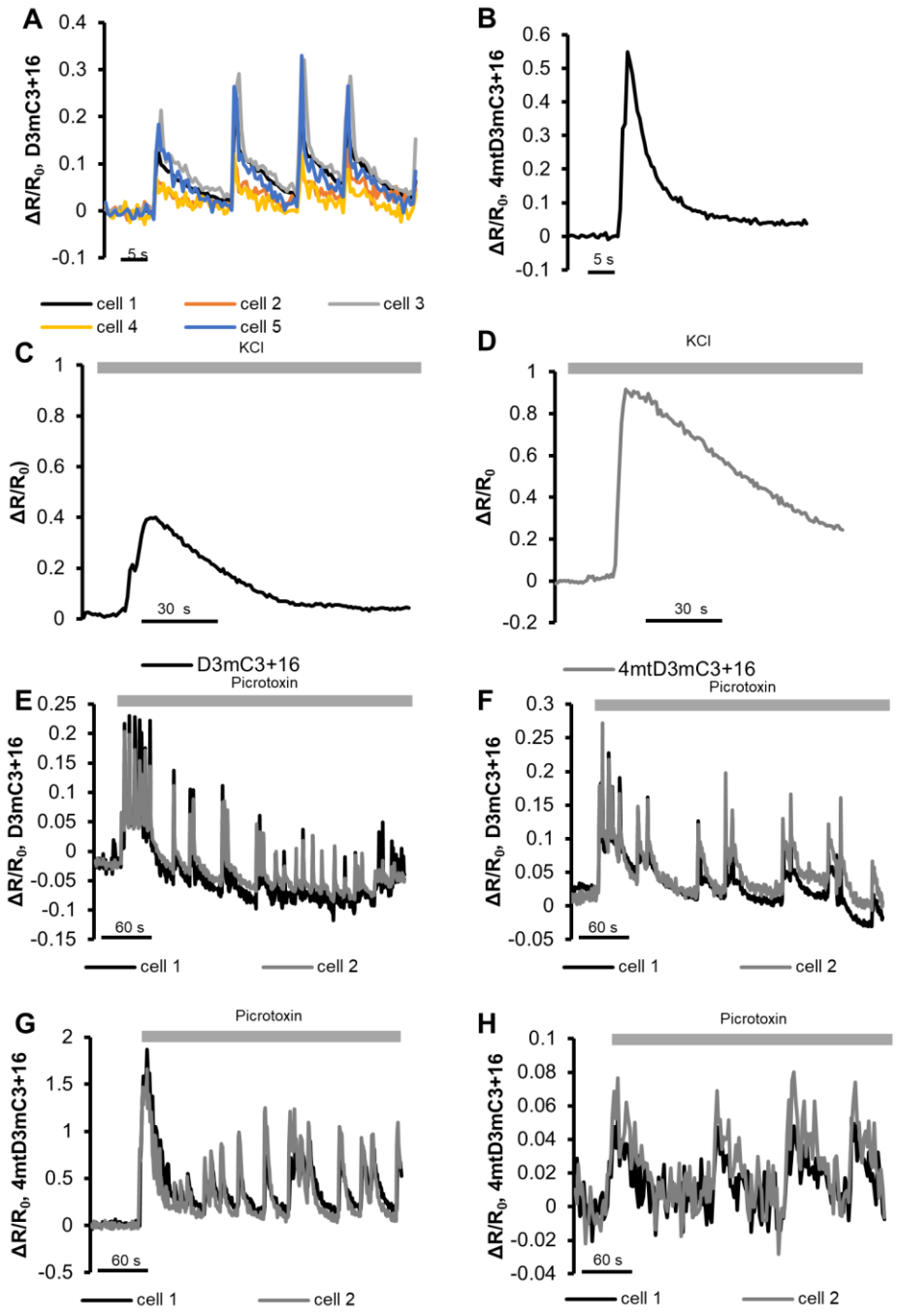
A
ΔR/R0, D3mC3+16
5 s
cell 1
cell 2
cell 3
cell 4
cell 5
B
ΔR/R0, 4mtD3mC3+16
5 s
C
KCl
ΔR/R0
30 s
D3mC3+16
D
KCl
ΔR/R0
30 s
4mtD3mC3+16
E
Picrotoxin
ΔR/R0, D3mC3+16
60 s
cell 1
cell 2
F
Picrotoxin
ΔR/R0, D3mC3+16
60 s
cell 1
cell 2
G
Picrotoxin
ΔR/R0, 4mtD3mC3+16
60 s
cell 1
cell 2
H
Picrotoxin
ΔR/R0, 4mtD3mC3+16
60 s
cell 1
cell 2

Figure S5. Related to Figure 5. *Monitoring [Ca^{2+}] changes in the brain: neonatal mice cortical and hippocampal neurons.* **(A-B)** Representative traces of spontaneous Ca^{2+} oscillations in primary cortical neurons infected with AAV9-syn-D3mC3+16 **(A)** or AAV9-syn-4mtD3mC3+16 **(B)**. Spontaneous activity was recorded in the cytosol of about 15% of the analyzed cells, while only more rarely a significant spontaneous rise in mitochondrial $[Ca^{2+}]_m$ has been observed. **(C-D)** Representative traces of Ca^{2+} rise induced by depolarization with 30 mM KCl in primary cortical neurons infected with AAV9-syn-D3mC3+16 **(C)** or AAV9-syn-4mtD3mC3+16 **(D)**. The rise in mitochondrial $\Delta R/R_0$ was about twofold larger than the rise in the cytosol. **(E-H)** Representative Ca^{2+} spikes induced by the GABA-A antagonist picrotoxin (PTX 50 µM, arrow) in primary neurons infected with AAV9-syn-D3mC3+16 from cortex **(E)** or hippocampus **(F)** or infected with AAV9-syn-4mtD3mC3+16 from cortex **(G)** or hippocampus **(H)**. Picrotoxin-induced oscillations were synchronous among different neurons in the same field of view, whether expressing the cytosolic or the mitochondrial probes. Data are plotted as $\Delta R/R_0$.

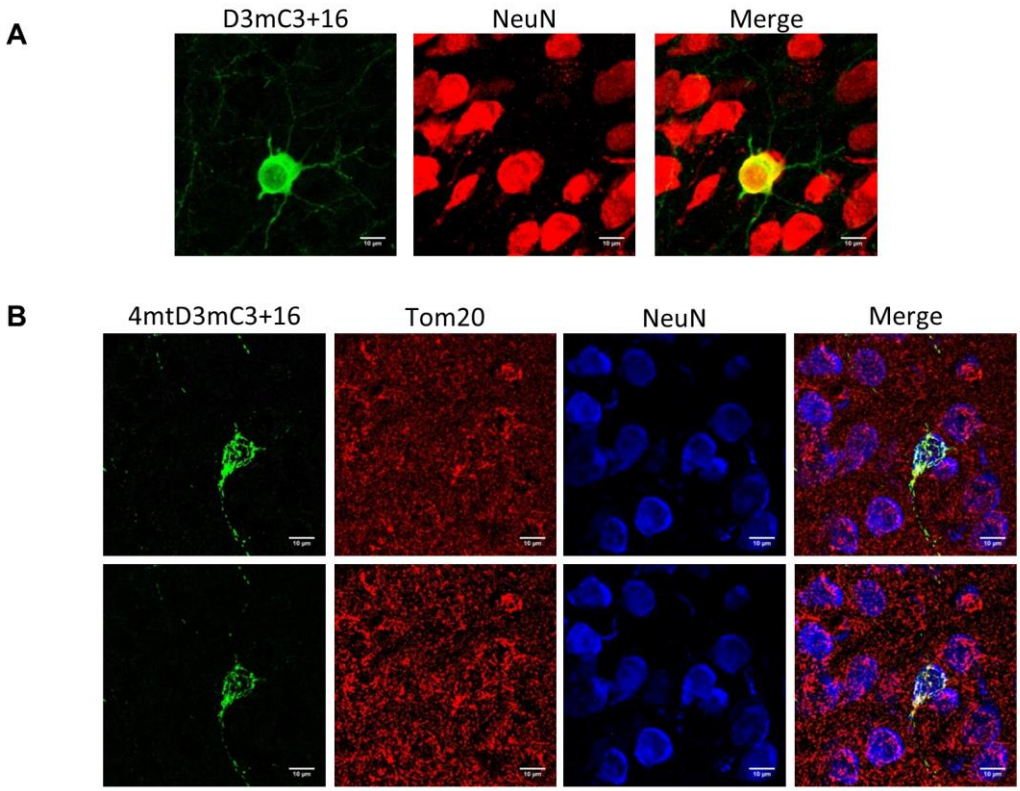

Figure S6. Related to Figure 5. *The mitochondrial and the cytosolic probes are properly localized ex vivo*. **(A)** The cytosolic localization of the probe in somatosensory cortex neurons from injected mice was assessed by immunohistochemistry. Yellow color indicates co-localization of D3mC3+16 and neurons, labeled with anti-NeuN antibody. **(B)** The mitochondrial localization of the probe in somatosensory cortex neurons from injected mice was evaluated for co-localization with a mitochondrial marker, TOM20 and for neurons as described in panel A. Yellow color indicates co-localization between mitochondria and 4mtD3mC3+16 in an infected neuron.

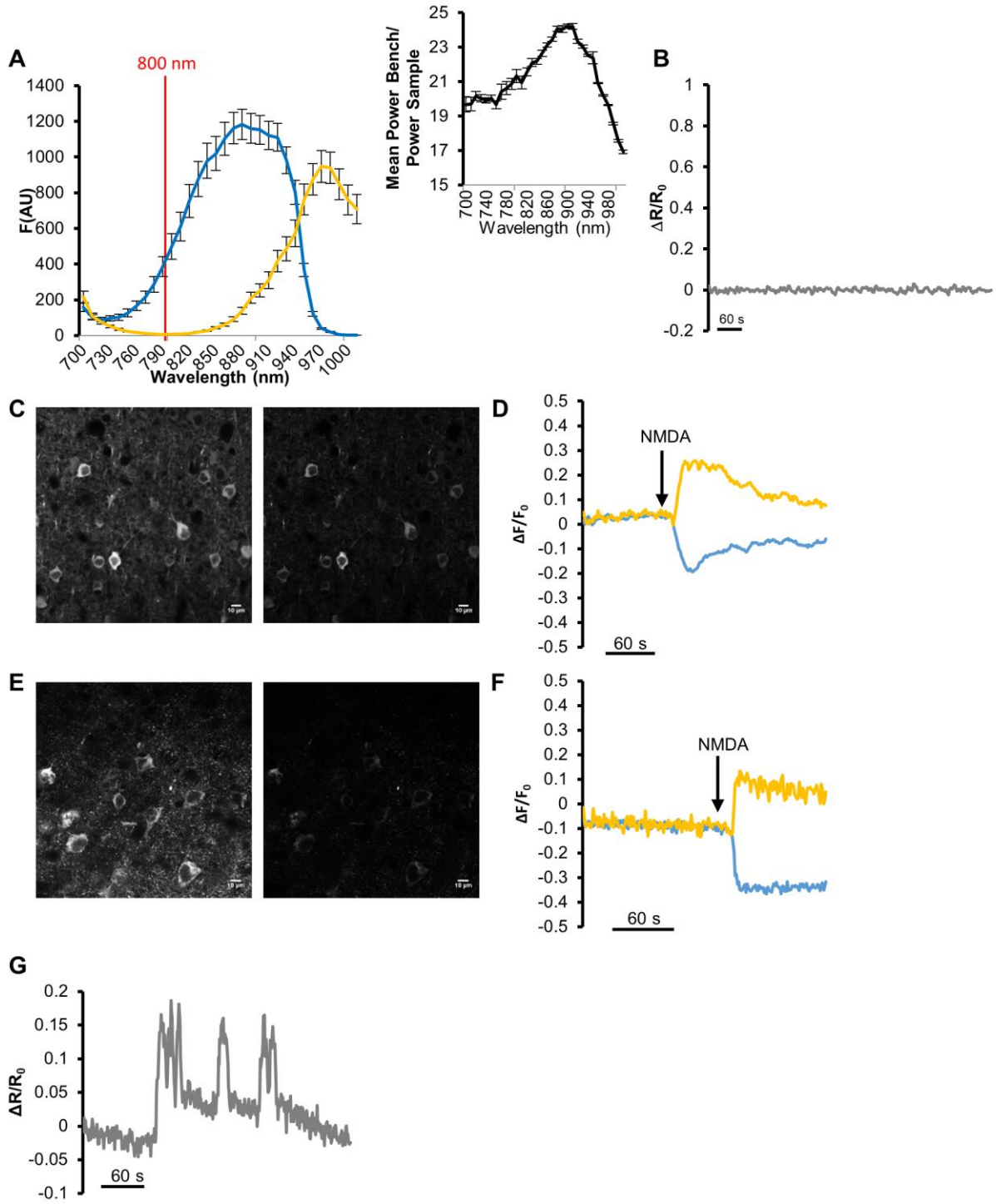

Figure S7. Related to Figure 5. *FRET two-photon microscopy.* **(A)** Two-photon excitation spectra of mCerulean3 (green) and cpV (yellow) transiently expressed in HeLa cells. The spectra were calculated for each sample as the mean fluorescence in a.u. (arbitrary unit) ±SEM. *Inset.* Laser power ratio in mW for each wavelength (700-1010 nm). The calibration allows performing the measurement

at a constant number of photons. The optimal two-photon excitation wavelength to minimize the cross-excitation of donor and acceptor was 800 nm. **(B)** Stability of the probe. Representative trace from neurons expressing 4mtD3mC3+16, illuminated at 1.53 Hz. No significant change in R was observed during 7 minutes of imaging. Data are presented as $\Delta R/R_0$. **(C)** Representative images of donor (*left*) and acceptor (*right*) channel using two-photon microscopy in slices from mice infected with AAV9-syn-D3mC3+16. Scale bar, 10 µm. **(D)** Individual traces of $\Delta F/F_0$ at 480/20 nm (mCerulean3 signal, cyan line) and 535/25 nm (cpV signal, orange line) in neurons expressing the D3mC3+16 from brain slice and stimulated with 1 mM NMDA in slices. **(E)** Representative images of donor (*left*) and acceptor (*right*) channel using two-photon microscope in slices from mice infected with AAV9-syn-4mtD3mC3+16. Scale bar, 10 µm. **(F)** Individual traces of $\Delta F/F_0$ at 480/20 nm (mCerulean3 signal, cyan line) and 535/25 nm (cpV signal, orange line) in neurons expressing the 4mtD3mC3+16 from brain slice and stimulated with 1 mM NMDA in slices, where indicated by the arrow. **(G)** Representative traces of spontaneous Ca^{2+} oscillations recorded in neurons from hippocampal slices from mice infected with AAV9-syn-D3mC3+16.

Sample	τ_1 (ns)	A_1	τ_2 (ns)	A_2	$\langle\tau\rangle$ (ns)
4mt-mCer3 pH 8.0	3.61 ± 0.02				
4mt-mCer3 pH 7.5	3.36 ± 0.01				
4mt-mCer3 pH 7.0	3.19 ± 0.04				
4mt-ECFP pH 8.0	**3.98 ± 0.16**	**49 ± 3 %**	**1.51 ± 0.09**	**51 ± 3 %**	**2.71 ± 0.06**
4mt-ECFP pH 7.5	3.14 ± 0.02	68 ± 1 %	1.08 ± 0.02	32 ± 1 %	2.48 ± 0.01
4mt-ECFP pH 7.0	3.07 ± 0.03	59 ± 1 %	1.13 ± 0.02	41 ± 1 %	2.29 ± 0.02

Table S1. **Related to Figure 3.** Donor average lifetimes ($<\tau>$) and relative amplitudes (A_i) obtained from the decay fitting of HeLa cells expressing 4mt-mCerulean3 (here indicated as 4mt-mCer3) or 4mt-CFP at pH equal to 8.0, 7.5 and 7.0 (N≥10).

4mtD3mC3+16, pH=8	τ_1 **(ns)**	A_1	τ_2 **(ns)**	A_2	$\langle\tau\rangle$ **(ns)**	E_{FRET} **%**
Ca_{min}	3.58 ± 0.03	72 ± 1 %	1.24 ± 0.05	28 ± 1 %	2.94 ± 0.01	**18**
[Ca^{2+}]=0.034 μM	3.66 ± 0.07	65 ± 2 %	1.30 ± 0.07	35 ± 1 %	2.84 ± 0.03	**21**
[Ca^{2+}]=3.5 μM	3.47 ± 0.04	68 ± 2 %	0.96 ± 0.04	32 ± 2 %	2.67 ± 0.04	**26**
[Ca^{2+}]=7.5 μM	3.40 ± 0.03	68 ± 1 %	0.90 ± 0.05	32 ± 2 %	2.59 ± 0.03	**28**
[Ca^{2+}]=10 μM	3.47 ± 0.07	69 ± 3 %	0.89 ± 0.04	31 ± 3 %	2.53 ± 0.05	**30**
[Ca^{2+}]=60 μM	3.34 ± 0.02	67 ± 2 %	0.73 ± 0.04	33 ± 2 %	2.48 ± 0.07	**31**
[Ca^{2+}=100 μM	3.21 ± 0.05	66 ± 1 %	0.66 ± 0.07	34 ± 1 %	2.33 ± 0.15	**36**
[Ca^{2+}]=500 μM	3.21 ± 0.05	65 ± 1 %	0.64 ± 0.05	35 ± 1 %	2.31 ± 0.06	**36**

Table S2. Related to Figure 3. Donor average lifetimes (<τ>) and relative amplitudes (A_i) obtained from the decay fitting of HeLa cells expressing 4mtD3mC3+16 (here indicated as 4mtD3mCer3+16) at pH 8.0 and at different [Ca^{2+}] concentrations. Data are presented as mean±SEM of N≥10 cells.

4mtD3cpv, pH=8	τ_1 (ns)	A_1	τ_2 (ns)	A_2	$\langle\tau\rangle$ (ns)	E_{FRET} %
Ca_{min}	2.89 ± 0.02	49 ± 1 %	0.88 ± 0.02	51 ± 1 %	1.86 ± 0.01	31
[Ca^{2+}]=0.034 μM	2.96 ± 0.03	42 ± 1 %	1.00 ± 0.02	57 ± 1 %	1.83 ± 0.01	32
[Ca^{2+}]=3.5 μM	2.84 ± 0.03	46 ± 1 %	0.84 ± 0.02	54 ± 1 %	1.75 ± 0.02	35
[Ca^{2+}]=7.5 μM	2.73 ± 0.03	46 ± 1 %	0.75 ± 0.02	54 ± 1 %	1.67 ± 0.02	38
[Ca^{2+}]=10 μM	2.77 ± 0.03	43 ± 1 %	0.84 ± 0.01	57 ± 1 %	1.66 ± 0.02	39
[Ca^{2+}]=20 μM	2.73 ± 0.02	45 ± 1 %	0.75 ± 0.01	55 ± 1 %	1.64 ± 0.01	39
[Ca^{2+}]=30 μM	2.74 ± 0.02	45 ± 1 %	0.75 ± 0.01	55 ± 1 %	1.64 ± 0.02	39
[Ca^{2+}]=60 μM	2.73 ± 0.03	45 ± 1 %	0.72 ± 0.01	55 ± 1 %	1.63 ± 0.03	40
[Ca^{2+}]=500 μM	2.66 ± 0.02	41 ± 1 %	0.73 ± 0.01	58 ± 1 %	1.53 ± 0.02	43

Table S3. Related to Figure 3. Donor average lifetimes (<τ>) and relative amplitudes (A_i) obtained from the decay fitting of HeLa cells expressing 4mtD3cpv at pH 8.0 and at different [Ca^{2+}] concentrations. Data are presented as mean±SEM of N≥10 cells. The decrease in the shorter donor lifetime (about 50% for 4mtD3mC3+16 and 17% for 4mtD3cpv) and increase in its relative amplitude A_2 (25% in 4mtD3mC3+16 and of 16% for 4mtD3cpv) upon increase in [Ca^{2+}], confirm the better performance of mCerulean3-based Cameleon compared to the original Cameleon (compare with **Table S2** for 4mtD3mC3+16).

4mtD3mC3+16, pH=7.5	τ_1 (ns)	A_1	τ_2 (ns)	A_2	$\langle\tau\rangle$ (ns)	E_{FRET} %
Ca_{min}	3.55 ± 0.03	61 ± 1 %	0.94 ± 0.03	39 ± 1 %	2.53 ± 0.03	25
[Ca^{2+}]=0.7 μM	3.52 ± 0.03	61 ± 1 %	0.87 ± 0.05	39 ± 1 %	2.48 ± 0.06	26
[Ca^{2+}]=10 μM	3.39 ± 0.03	60 ± 2 %	0.75 ± 0.03	40 ± 2 %	2.34 ± 0.08	30
[Ca^{2+}]=50 μM	3.37 ± 0.03	61 ± 1 %	0.78 ± 0.02	39 ± 2 %	2.34 ± 0.05	30
[Ca^{2+}]=100 μM	3.53 ± 0.03	61 ± 1 %	0.79 ± 0.03	39 ± 1 %	2.47 ± 0.06	26
[Ca^{2+}]=500 μM	3.45 ± 0.03	60 ± 2 %	0.74 ± 0.04	40 ± 2 %	2.37 ± 0.09	29

4mtD3mC3+16, pH=7, ROIs with Rise	τ_1 (ns)	A_1	τ_2 (ns)	A_2	$\langle\tau\rangle$ (ns)
Ca_{min}	3.58 ± 0.08	61 ± 1 %	0.95 ± 0.12	39 ± 1 %	2.54 ± 0.10
[Ca^{2+}]=0.7 μM	3.43 ± 0.02	60 ± 2 %	0.70 ± 0.01	40 ± 2 %	2.34 ± 0.06
[Ca^{2+}]=10 μM	3.47 ± 0.02	60 ± 2 %	0.73 ± 0.02	40 ± 2 %	2.38 ± 0.08
[Ca^{2+}]=50 μM	3.47 ± 0.09	64 ± 3 %	0.80 ± 0.11	36 ± 3 %	2.52 ± 0.18
[Ca^{2+}]=100 μM	3.46 ± 0.05	57 ± 1 %	0.70 ± 0.03	43 ± 1 %	2.27 ± 0.06
[Ca^{2+}]=500 μM	3.46 ± 0.03	56 ± 2 %	0.68 ± 0.02	44 ± 2 %	2.22 ± 0.07

4mtD3mC3+16, pH=7, ROIs without Rise	τ_1 (ns)	A_1	τ_2 (ns)	A_2	$\langle\tau\rangle$ (ns)
Ca_{min}	3.23 ± 0.06	49 ± 3 %	0.65 ± 0.06	51 ± 3 %	1.91 ± 0.15
[Ca^{2+}]=0.7 μM	3.28 ± 0.03	49 ± 1 %	0.59 ± 0.03	51 ± 1 %	1.92 ± 0.05
[Ca^{2+}]=10 μM	3.31 ± 0.11	51 ± 6 %	0.56 ± 0.01	49 ± 6 %	1.98 ± 0.22
[Ca^{2+}]=50 μM	3.24 ± 0.10	56 ± 2 %	0.52 ± 0.10	44 ± 2 %	2.05 ± 0.10
[Ca^{2+}]=100 μM	3.24 ± 0.06	49 ± 1 %	0.56 ± 0.04	51 ± 1 %	1.88 ± 0.06
[Ca^{2+}]=500 μM	3.40 ± 0.03	52 ± 2 %	0.60 ± 0.03	48 ± 2 %	2.10 ± 0.10

Table S4. Related to Figure 3. Donor average lifetimes (<τ>) and relative amplitudes (A_i) obtained from the decay fitting of HeLa cells expressing 4mtD3mC3+16 at pH 7.5 or 7 and at different [Ca^{2+}] concentrations. Grey box includes the values before the saturation limit: above this limit the sensor is almost insensitive to further increase of [Ca^{2+}]. Data are presented as mean±SEM of N≥10 cells. The data collected at pH 7.0 are divided into two groups, depending on the presence or absence of the rise component in the decay recorded on acceptor channel detection. They are respectively called "ROIs with Rise" and "ROIs without Rise". Grey boxes include the values before the saturation limit: above this limit the sensor is almost insensitive to further increase of [Ca^{2+}]. In almost half the cells at pH 7.0 and low [Ca^{2+}] the rise component in the acceptor decay is not evident. The absence of the rise term does not result in an increase in the ratio between the emission intensity collected in the acceptor channel toward the emission in the donor channel (data not shown), even if the donor average lifetime is reduced. Despite we do not have a clear explanation of this phenomenon, we can hypothesize that the energy transfer process is strongly affected by the pH effect on donor lifetime, causing an underestimation of the Ca^{2+}-dependent FRET efficiency at acidic pH. Generally, pH acidification causes a large drop in FRET efficiency that is however not paralleled by the ability of the probe to report small changes in [Ca^{2+}] up to 10-20 μM (see also **Table S5. Related to Figure 3** for 4mtD3cpv), as those induced by MCUC protein levels' manipulation. Data are presented as mean±SEM of N≥10 cells.

4mtD3cpv, pH=7.5	τ_1 (ns)	A_1	τ_2 (ns)	A_2	$\langle\tau\rangle$ (ns)	E_{FRET} %
Ca_{min}	2.84 ± 0.01	44 ± 1 %	0.75 ± 0.02	55 ± 1 %	1.68 ± 0.02	32
[Ca^{2+}]=0.7 μM	2.79 ± 0.02	43 ± 1 %	0.71 ± 0.02	57 ± 1 %	1.61 ± 0.03	35
[Ca^{2+}]=10 μM	2.75 ± 0.02	43 ± 1 %	0.71 ± 0.02	57 ± 1 %	1.58 ± 0.02	36
[Ca^{2+}]=50 μM	2.77 ± 0.02	44 ± 1 %	0.69 ± 0.03	56 ± 1 %	1.61 ± 0.03	35
[Ca^{2+}]=100 μM	2.73 ± 0.02	43 ± 1 %	0.68 ± 0.02	57 ± 1 %	1.56 ± 0.02	37
[Ca^{2+}]=500 μM	2.75 ± 0.02	43 ± 1 %	0.69 ± 0.01	57 ± 1 %	1.57 ± 0.03	37

4mtD3cpv, pH=7, ROIs with Rise	τ_1 (ns)	A_1	τ_2 (ns)	A_2	$\langle\tau\rangle$ (ns)
Ca_{min}	2.74 ± 0.02	42 ± 1 %	0.70 ± 0.02	58 ± 1 %	1.55 ± 0.02
[Ca^{2+}]=0.7 μM	2.76 ± 0.03	43 ± 1 %	0.74 ± 0.02	57 ± 1 %	1.61 ± 0.02
[Ca^{2+}]=10 μM	2.74 ± 0.02	43 ± 2 %	0.70 ± 0.01	57 ± 2 %	1.58 ± 0.02
[Ca^{2+}]=50 μM	2.74 ± 0.01	40 ± 1 %	0.68 ± 0.02	60 ± 1 %	1.51 ± 0.02
[Ca^{2+}]=100 μM	2.74 ± 0.05	40 ± 2 %	0.67 ± 0.02	60 ± 2 %	1.50 ± 0.06
[Ca^{2+}]=500 μM	2.71 ± 0.03	40 ± 1 %	0.62 ± 0.03	60 ± 1 %	1.46 ± 0.03

4mtD3cpv, pH=7, ROIs without Rise	τ_1 (ns)	A_1	τ_2 (ns)	A_2	$\langle\tau\rangle$ (ns)
Ca_{min}	2.63 ± 0.06	36 ± 2 %	0.60 ± 0.03	64 ± 2 %	1.34 ± 0.08
[Ca^{2+}]=0.7 μM	2.62 ± 0.03	38 ± 1 %	0.59 ± 0.01	62 ± 1 %	1.35 ± 0.03
[Ca^{2+}]=10 μM	2.55 ± 0.04	32 ± 3 %	0.53 ± 0.03	68 ± 3 %	1.18 ± 0.07
[Ca^{2+}]=50 μM	2.62 ± 0.01	38 ± 1 %	0.59 ± 0.10	62 ± 1 %	1.36 ± 0.01
[Ca^{2+}]=100 μM	2.61 ± 0.03	36 ± 1 %	0.52 ± 0.03	64 ± 1 %	1.28 ± 0.03
[Ca^{2+}]=500 μM	2.65 ± 0.03	38 ± 1 %	0.60 ± 0.03	62 ± 1 %	1.37 ± 0.03

Table S5. Related to Figure 3. Donor average lifetimes (<τ>) and relative amplitudes (A_i) obtained from the decay fitting of HeLa cells expressing 4mtD3cpv at pH 7.5 or 7 and at different [Ca^{2+}] concentrations. Grey box includes the values before the saturation limit: above this limit the sensor is almost insensitive to further increase of [Ca^{2+}]. Data are presented as mean±SEM of N≥10 cells.
The data collected at pH 7.0 are divided into two groups, depending on the presence or absence of the rise component in the decay recorded on acceptor channel detection. They are respectively called "ROIs with Rise" and "ROIs without Rise". Almost half the cells at pH 7.0 and low [Ca^{2+}] the rise component in the acceptor decay is not evident.

4mtD3mC3+16	N_ ROIs (N%)	τ_1 (ns)	A_1	τ_2 (ns)	A_2	$\langle\tau\rangle$ (ns)
Ctrl, ROIs with Rise	37 (80%)	3.41 ± 0.04	61 ± 1 %	1.07 ± 0.05	39 ± 1 %	2.51 ± 0.02
ROIs without Rise	9 (20%)	3.16 ± 0.02	60 ± 1 %	0.76 ± 0.07	40 ± 1 %	2.21 ± 0.04
MICU1, ROIs with Rise	10 (40%)	3.38 ± 0.05	62 ± 1 %	0.98 ± 0.06	38 ± 1 %	2.47 ± 0.06
ROIs without Rise	15 (60%)	3.27 ± 0.04	54 ± 3 %	0.78 ± 0.05	47 ± 3 %	2.09 ± 0.10
MCU, ROIs with Rise	44 (96%)	3.32 ± 0.03	60 ± 1 %	0.99 ± 0.03	40 ± 1 %	2.39 ± 0.03
ROIs without Rise	3 (6%)	2.78 ± 0.22	38 ± 8 %	0.63 ± 0.04	62 ± 8 %	1.48 ± 0.28
MICU1+MCU, ROIs with Rise	18 (56%)	3.29 ± 0.03	60 ± 1 %	0.93 ± 0.04	40 ± 1 %	2.35 ± 0.04
ROIs without Rise	14 (44%)	3.20 ± 0.02	51 ± 2 %	0.73 ± 0.02	49 ± 2 %	1.99 ± 0.06

Table S6. Related to Figure 3. Donor average lifetimes ($<\tau>$) and relative amplitudes (A_i) obtained from the decay fitting of HeLa cells expressing 4mtD3mC3+16 and overexpressing MCU, MICU1 and MICU1+MCU. The Ctrl condition refers to basal [Ca^{2+}] in HeLa cells transfected with void vector. For each condition, the analyzed cells are divided into two groups, depending on the presence or absence of the rise term in the acceptor decay curve. N_ROIs is the number of cells considered for each group and used for the calculation of the mean values reported in the table.

D3mC3+16

```
gccaccatggtgagcaagggcgaggagctgttcaccggggtggtgcccatcctggtcgag
 A  T  M  V  S  K  G  E  E  L  F  T  G  V  V  P  I  L  V  E
ctggacggcgacgtaaacggccacaagttcagcgtgtccggcgagggcgagggcgatgcc
 L  D  G  D  V  N  G  H  K  F  S  V  S  G  E  G  E  G  D  A
acctacggcaagctgaccctgaagttcatctgcaccaccggcaagctgcccgtgccctgg
 T  Y  G  K  L  T  L  K  F  I  C  T  T  G  K  L  P  V  P  W
cccaccctcgtgaccaccctgagctggggcgtgcagtgcttcgcccgctaccccgaccac
 P  T  L  V  T  T  L  S  W  G  V  Q  C  F  A  R  Y  P  D  H
atgaagcagcacgacttcttcaagtccgccatgcccgaaggctacgtccaggagcgcacc
 M  K  Q  H  D  F  F  K  S  A  M  P  E  G  Y  V  Q  E  R  T
atcttcttcaaggacgacggcaactacaagacccgcgccgaggtgaagttcgagggcgac
 I  F  F  K  D  D  G  N  Y  K  T  R  A  E  V  K  F  E  G  D
accctggtgaaccgcatcgagctgaagggcatcgacttcaaggaggacggcaacatcctg
 T  L  V  N  R  I  E  L  K  G  I  D  F  K  E  D  G  N  I  L
gggcacaagctggagtacaacgccatccacggcaacgtctatatcaccgccgacaagcag
 G  H  K  L  E  Y  N  A  I  H  G  N  V  Y  I  T  A  D  K  Q
aagaacggcatcaaggccaacttcggcctcaactgcaacatcgaggacggcagcgtgcag
 K  N  G  I  K  A  N  F  G  L  N  C  N  I  E  D  G  S  V  Q
ctcgccgaccactaccagcagaacacccccatcggcgacggccccgtgctgctgcccgac
 L  A  D  H  Y  Q  Q  N  T  P  I  G  D  G  P  V  L  L  P  D
aaccactacctgagcacccagtccaagctgagcaaagaccccaacgagaagcgcgatcac
 N  H  Y  L  S  T  Q  S  K  L  S  K  D  P  N  E  K  R  D  H
atggtcctgctggagttcgtgaccgccgccgggatcactctcggcatggacgagctgtac
 M  V  L  L  E  F  V  T  A  A  G  I  T  L  G  M  D  E  L  Y
aagcgcatgcatgaccagctgaccgaggaacagatcgccgagttcaaagaggccttcagc
 K  R  M  H  D  Q  L  T  E  E  Q  I  A  E  F  K  E  A  F  S
ctgctggacaaggacggcgacggcaccatcaccaccaaagagctgggcaccgccctgaga
 L  L  D  K  D  G  D  G  T  I  T  T  K  E  L  G  T  A  L  R
agcctgggccagaatcctacagaggccgagctgcaggacatgatcaacgaggtggacgcc
 S  L  G  Q  N  P  T  E  A  E  L  Q  D  M  I  N  E  V  D  A
gacggcaacggcacaatctacttccccgagttcctgaccatgatggccagaaagatgaag
 D  G  N  G  T  I  Y  F  P  E  F  L  T  M  M  A  R  K  M  K
gacaccgacagcgaggaagagatccgcgaggccttccgggtgttcgataaggacggaaac
 D  T  D  S  E  E  E  I  R  E  A  F  R  V  F  D  K  D  G  N
ggctacatctctgccgccgagctgagacacgtgatgaccaacctgggcgagaagctgacc
 G  Y  I  S  A  A  E  L  R  H  V  M  T  N  L  G  E  K  L  T
gacgaagaggtggacgagatgatcagagaggccgacatcgacggggacggccaggtcaac
 D  E  E  V  D  E  M  I  R  E  A  D  I  D  G  D  G  Q  V  N
tacgaggaattcgtgcagatgatgaccgccaagggcggcggcggcggcggcggcggcggc
 Y  E  E  F  V  Q  M  M  T  A  K  G  G  G  G  G  G  G  G  G
ggcggcggcggcggcggcggcggcagcaagagaagatggcagaaaaccggtcacgccgtg
 G  G  G  G  G  G  G  G  S  K  R  R  W  Q  K  T  G  H  A  V
cgggccttcggcagactgaagaagatcagcagctctggcgccctggagctcatggatggc
 R  A  F  G  R  L  K  K  I  S  S  S  G  A  L  E  L  M  D  G
ggagtccagctggctgatcattatcagcagaatactcccatcggagatggaccagtcctg
 G  V  Q  L  A  D  H  Y  Q  Q  N  T  P  I  G  D  G  P  V  L
ctgcccgataatcactatctgtcctaccagtccgccctgtccaaggaccctaatgagaaa
 L  P  D  N  H  Y  L  S  Y  Q  S  A  L  S  K  D  P  N  E  K
cgcgatcatatggtcctgctcgaatttgtcacagctgccggcatcaccctgggcatggac
 R  D  H  M  V  L  L  E  F  V  T  A  A  G  I  T  L  G  M  D
gagctgtacaagggcggctctggcggcatggtgtccaaggggaagaactctttacaggg
 E  L  Y  K  G  G  S  G  G  M  V  S  K  G  E  E  L  F  T  G
gtggtgcctattctggtcgagctggacggggatgtgaacggacacaagttctccgtgtct
 V  V  P  I  L  V  E  L  D  G  D  V  N  G  H  K  F  S  V  S
ggggagggcgaggggatgctacctatggcaagctgacactgaaactgatctgtaccaca
```

```
 G  E  G  E  G  D  A  T  Y  G  K  L  T  L  K  L  I  C  T  T
gggaagctcccagtgccctggcccacactcgtgaccacactgggatacggcctgcagtgt
 G  K  L  P  V  P  W  P  T  L  V  T  T  L  G  Y  G  L  Q  C
tttgcccgctaccctgatcatatgaagcagcatgatttttttcaaatccgctatgcctgag
 F  A  R  Y  P  D  H  M  K  Q  H  D  F  F  K  S  A  M  P  E
ggatatgtccaggaacggacaatcttctttaaggatgatgggaattataagacacgggct
 G  Y  V  Q  E  R  T  I  F  F  K  D  D  G  N  Y  K  T  R  A
gaagtcaagtttgaggggggataccctcgtgaatcggatcgaactgaaggggattgatttc
 E  V  K  F  E  G  D  T  L  V  N  R  I  E  L  K  G  I  D  F
aaagaggacgggaatattctcggacataagctggagtataattacaactctcacaatgtc
 K  E  D  G  N  I  L  G  H  K  L  E  Y  N  Y  N  S  H  N  V
tacatcacagctgataagcagaaaaatgggattaaggctaactttaagatccgccacaat
 Y  I  T  A  D  K  Q  K  N  G  I  K  A  N  F  K  I  R  H  N
atcgagtaa
 I  E  -
```

4mtD3mC3+16

```
gccaccatgagcgtgctgacacccctgctgctgagaggcctgacaggcagcgctagaagg
 A  T  M  S  V  L  T  P  L  L  L  R  G  L  T  G  S  A  R  R
ctgcctgtgcccagagccaagatccacagcctgcctccagaggggccatggtccgtgctg
 L  P  V  P  R  A  K  I  H  S  L  P  P  E  G  P  W  S  V  L
actcctctgctcctgcggggactgacaggctctgctcggagactgccagtgcctcgggct
 T  P  L  L  L  R  G  L  T  G  S  A  R  R  L  P  V  P  R  A
aagatccactccctgccacctgagggcggttcctctgtcctgactccactcctgctcaga
 K  I  H  S  L  P  P  E  G  G  S  S  V  L  T  P  L  L  L  R
ggactgaccggatctgccagacggctgccagtccccagggccaaaattcactctctgcct
 G  L  T  G  S  A  R  R  L  P  V  P  R  A  K  I  H  S  L  P
cccgaaggcggctctgtgctcacaccactgctcctcaggggctgactggaagcgcacgc
 P  E  G  G  S  V  L  T  P  L  L  L  R  G  L  T  G  S  A  R
agactgcctgtcccacgcgcaaagattcattccctgccccccgagggaccatggggatcc
 R  L  P  V  P  R  A  K  I  H  S  L  P  P  E  G  P  W  G  S
gtgagcaagggcgaggagctgttcaccggggtggtgcccatcctggtcgagctggacggc
 V  S  K  G  E  E  L  F  T  G  V  V  P  I  L  V  E  L  D  G
gacgtaaacggccacaagttcagcgtgtccggcgagggcgagggcgatgccacctacggc
 D  V  N  G  H  K  F  S  V  S  G  E  G  E  G  D  A  T  Y  G
aagctgaccctgaagttcatctgcaccaccggcaagctgcccgtgccctggcccaccctc
 K  L  T  L  K  F  I  C  T  T  G  K  L  P  V  P  W  P  T  L
gtgaccaccctgagctggggcgtgcagtgcttcgcccgctaccccgaccacatgaagcag
 V  T  T  L  S  W  G  V  Q  C  F  A  R  Y  P  D  H  M  K  Q
cacgacttcttcaagtccgccatgcccgaaggctacgtccaggagcgcaccatcttcttc
 H  D  F  F  K  S  A  M  P  E  G  Y  V  Q  E  R  T  I  F  F
aaggacgacggcaactacaagacccgcgccgaggtgaagttcgagggcgacaccctggtg
 K  D  D  G  N  Y  K  T  R  A  E  V  K  F  E  G  D  T  L  V
aaccgcatcgagctgaagggcatcgacttcaaggaggacggcaacatcctggggcacaag
 N  R  I  E  L  K  G  I  D  F  K  E  D  G  N  I  L  G  H  K
ctggagtacaacgccatccacggcaacgtctatatcaccgccgacaagcagaagaacggc
 L  E  Y  N  A  I  H  G  N  V  Y  I  T  A  D  K  Q  K  N  G
atcaaggccaacttcggcctcaactgcaacatcgaggacggcagcgtgcagctcgccgac
 I  K  A  N  F  G  L  N  C  N  I  E  D  G  S  V  Q  L  A  D
cactaccagcagaacaccccatcggcgacggccccgtgctgctgcccgacaaccactac
 H  Y  Q  Q  N  T  P  I  G  D  G  P  V  L  L  P  D  N  H  Y
ctgagcacccagtccaagctgagcaaagaccccaacgagaagcgcgatcacatggtcctg
 L  S  T  Q  S  K  L  S  K  D  P  N  E  K  R  D  H  M  V  L
ctggagttcgtgaccgccgccgggatcactctcggcatggacgagctgtacaagcgcatg
 L  E  F  V  T  A  A  G  I  T  L  G  M  D  E  L  Y  K  R  M
```

```
catgaccagctgaccgaggaacagatcgccgagttcaaagaggccttcagcctgctggac
 H  D  Q  L  T  E  E  Q  I  A  E  F  K  E  A  F  S  L  L  D
aaggacggcgacggcaccatcaccaccaaagagctgggcaccgccctgagaagcctgggc
 K  D  G  D  G  T  I  T  T  K  E  L  G  T  A  L  R  S  L  G
cagaatcctacagaggccgagctgcaggacatgatcaacgaggtggacgccgacggcaac
 Q  N  P  T  E  A  E  L  Q  D  M  I  N  E  V  D  A  D  G  N
ggcacaatctacttccccgagttcctgaccatgatggccagaaagatgaaggacaccgac
 G  T  I  Y  F  P  E  F  L  T  M  M  A  R  K  M  K  D  T  D
agcgaggaagagatccgcgaggccttccgggtgttcgataaggacggaaacggctacatc
 S  E  E  E  I  R  E  A  F  R  V  F  D  K  D  G  N  G  Y  I
tctgccgccgagctgagacacgtgatgaccaacctgggcgagaagctgaccgacgaagag
 S  A  A  E  L  R  H  V  M  T  N  L  G  E  K  L  T  D  E  E
gtggacgagatgatcagagaggccgacatcgacggggacggccaggtcaactacgaggaa
 V  D  E  M  I  R  E  A  D  I  D  G  D  G  Q  V  N  Y  E  E
ttcgtgcagatgatgaccgccaagggcggcggcggcggcggcggcggcggcggcggcggc
 F  V  Q  M  M  T  A  K  G  G  G  G  G  G  G  G  G  G  G  G
ggcggcggcggcggcagcaagagaagatggcagaaaaccggtcacgccgtgcgggccttc
 G  G  G  G  G  S  K  R  R  W  Q  K  T  G  H  A  V  R  A  F
ggcagactgaagaagatcagcagctctggcgccctggagctcatggatggcggagtccag
 G  R  L  K  K  I  S  S  S  G  A  L  E  L  M  D  G  G  V  Q
ctggctgatcattatcagcagaatactcccatcggagatggaccagtcctgctgcccgat
 L  A  D  H  Y  Q  Q  N  T  P  I  G  D  G  P  V  L  L  P  D
aatcactatctgtcctaccagtccgccctgtccaaggaccctaatgagaaacgcgatcat
 N  H  Y  L  S  Y  Q  S  A  L  S  K  D  P  N  E  K  R  D  H
atggtcctgctcgaatttgtcacagctgccggcatcaccctgggcatggacgagctgtac
 M  V  L  L  E  F  V  T  A  A  G  I  T  L  G  M  D  E  L  Y
aagggcggctctggcggcatggtgtccaaggggaagaactctttacaggggtggtgcct
 K  G  G  S  G  G  M  V  S  K  G  E  E  L  F  T  G  V  V  P
attctggtcgagctggacggggatgtgaacggacacaagttctccgtgtctggggagggc
 I  L  V  E  L  D  G  D  V  N  G  H  K  F  S  V  S  G  E  G
gaggggatgctacctatggcaagctgacactgaaactgatctgtaccacagggaagctc
 E  G  D  A  T  Y  G  K  L  T  L  K  L  I  C  T  T  G  K  L
ccagtgccctggcccacactcgtgaccacactgggatacggcctgcagtgttttgcccgc
 P  V  P  W  P  T  L  V  T  T  L  G  Y  G  L  Q  C  F  A  R
taccctgatcatatgaagcagcatgatttttttcaaatccgctatgcctgagggatatgtc
 Y  P  D  H  M  K  Q  H  D  F  F  K  S  A  M  P  E  G  Y  V
caggaacggacaatcttctttaaggatgatgggaattataagacacgggctgaagtcaag
 Q  E  R  T  I  F  F  K  D  D  G  N  Y  K  T  R  A  E  V  K
tttgaggggggataccctcgtgaatcggatcgaactgaaggggattgatttcaaagaggac
 F  E  G  D  T  L  V  N  R  I  E  L  K  G  I  D  F  K  E  D
gggaatattctcggacataagctggagtataattacaactctcacaatgtctacatcaca
 G  N  I  L  G  H  K  L  E  Y  N  Y  N  S  H  N  V  Y  I  T
gctgataagcagaaaaatgggattaaggctaactttaagatccgccacaatatcgagtaa
 A  D  K  Q  K  N  G  I  K  A  N  F  K  I  R  H  N  I  E  -
```

Table S7. Related to Figure 1.
Nucleotides and aminoacids sequence of the mCerulean3-based Cameleons.

Video S1. Related to Figure 1. Histamine stimulated mitochondrial Ca^{2+} uptake in HeLa cells.
The video shows the increase in the mitochondrial [Ca^{2+}] induced by histamine perfusion of Hela cells expressing 4mtD3mC3+16. The mitochondrial Ca^{2+} uptake is visualized employing a pseudo-colored scale that starts from blue-green, low [Ca^{2+}], and turns to yellow-red, high [Ca^{2+}].

Transparent methods

Contact for Reagent and Resource Sharing

Further information and requests for resources and reagents should be directed to and will be fulfilled by the First Author, Elisa Greotti (elisa.greotti@unipd.it).

Experimental Models

Animals

All procedures were conducted in accordance with the Italian and European Communities Council Directive on Animal Care and were approved by the Italian Ministry of Health (OPBA n 387/2018/PR, 26/02/2018 and 287/2015-PR, 05/03/15; authorization D2784.N.HEH, 03/07/18). We used C57BL/6J mice (both sexes) at postnatal days 15–20 (young) and ≥2 months old (adults).

Cell Culture and Transfection

- HeLa cells

HeLa cells were grown in Dulbecco's Modified Eagles medium (DMEM) containing 10% Fetal Calf Serum, supplemented with L-glutamine (2 mM), penicillin (100 U/ml) and streptomycin (100 µg/ml), in a humidified atmosphere containing 5% CO2. Cells were seeded onto glass coverslips (18 mm diameter for FRET, TMRM and mt-SypHer measurements and 24 mm for FLIM) and transfection was performed at 60% confluence using TransIT®-LT1 transfection reagent (Mirus Bio LLC) with 1 µg of DNA in 13- or 18-mm coverslips, 2 µg in 24-mm coverslips. Fluorescence, lifetime and confocal imaging were usually performed 24-48 hours after transfection.

- MEFs cells

MEFs were grown in DMEM supplemented with; 10% FCS, 1× nonessential amino acids, 1 mM L-glutamine, penicillin/streptomycin in a humidified atmosphere containing 5% CO2. Cells were seeded onto glass coverslips (13-mm or 24-mm diameter) and transfection was performed at 60% confluence using Lipofectamine™ 2000 Transfection Reagent (Life Technologies). Aequorin and FRET measurements were usually performed 24 h after transfection.

Primary cultures

- Neonatal cortical and hippocampal neurons

Primary cortical or hippocampal neurons were obtained from 0-1 day newborn mice (4-6 pups). Cells from mice neonatal cortices were dissociated in trypsin (0.8 mg/ml) for 10 min at 37 °C and digestion

was blocked by the trypsin inhibitor (6.3 µg/ml) plus DNAse I (40 µg/ml). Cells were gently suspended in pre-warmed supplemented Minimum Essential Media (MEM; in mM: 20 glucose, 0.5 L-glutamine, 0.0036 biotin, 1 pyruvic acid, also containing 1% N2 supplement, 0.5% B27 supplement, 25 µg/ml penicillin, 25 µg/ml streptomycin, 50 µg/ml neomycin and 10% horse serum). Cells were seeded on poly-L-lysine (100 µg/ml) for cortical or poly-L-lysine (30 µg/ml) and laminin (2 µg/ml) for hippocampal neurons coated glass coverslips of 18-mm diameter at a density of 0.5 x 10^6 cells/coverslip. After 24 h, the growth medium was replaced with serum- and antibiotic- free Neurobasal-A medium, containing B27 (2%) and L-glutamine (0.5 mM).

- Neonatal cardiomyocytes

Cultures of cardiomyocytes were prepared from ventricles of rats (0–3 days after birth). The heart was removed and rapidly placed in ice-cold HEPES-buffered saline containing in mM: 116 NaCl, 0.8 NaH_2PO_4, 5.3 KCl, 0.4 $MgSO_4$, 5 glucose and 20 HEPES, pH 7.4. Atria were discarded and ventricles were submitted to four subsequent digestions with 0.45 mg/ml collagenase and 5% pancreatin. The first supernatant containing cell debris and blood cells was discarded. Cell suspensions from the three subsequent digestions (20 min each) were centrifuged and the pellet was re-suspended in 2 ml of newborn calf serum. Cells were pooled and re-suspended in a complete medium DMEM/Medium 199 (4:1) supplemented with 2 mM glutamine, 100 U/ml penicillin, 100 mg/ml streptomycin, 5% newborn calf serum and 10% horse serum. Cells were then incubated for 1 hours at 37°C, allowing for a selective attachment of non-myocytes. The unattached cells were plated at a density of 0.6×10^6 cell/ml onto 18 mm diameter coverslips coated with laminin (1 µg/cm2).

- Human induced pluripotent stem cell (hiPSCs) culture.

hiPS cells were maintained in Essential 8 Flex Medium (ThermoFisher Scientific) on 1:100 Geltrex LDEV-Free Reduced Growth Factor Basement Membrane Matrix (ThermoFisher Scientific) and passaged every 4 days using 0.5 mM EDTA (Ethylenediaminetetraacetic acid, Life Technologies) in Dulbecco's PBS (DPBS) without Ca^{2+} or Mg^{2+} (Life Technologies) for 5 min at 37 degrees 5% CO_2/air environment. Cells were expanded in 6-well plates by passaging 1:8.

- Differentiation of iPSC into CMs.

The hiPS cells were differentiated into cardiomyocytes (CMs) using a direct differentiation method trough the STEMdiff Cardiomyocyte Differentiation Kit (Stemcell Technologies). Briefly, iPSC were plated at the density of 3.5 x 10^5 /well in a 12 well plate. After reaching 90% confluence, hiPSC were incubated with the induction media A for the mesodermal commitment. Two days after, cardiac

mesoderm commitment was achieved by the addition of medium B. 48h hours later, the medium was replaced with medium C for the cardiac induction and cells have been differentiated for 4 days. In the final step, the induction media C was replaced with maintenance media and cells were re-fed every other day, with spontaneously beating cells usually first appearing on Day 7 and robust contracting syncytium by Day 10.

Method Details

Constructs generation

D3mC3+16 and 4mtD3mC3+16

mCerulean3 was kindly gifted by Rizzo M. A. (Department of Physiology, University of Maryland School of Medicine, Baltimore, Maryland, United States of America). ECFP has been substituted inserting mCerulean3 cDNA between KpnI and SphI sites in D3cpv-pcDNA3. Restriction sites have been generated by PCR using specific primers:

5'-CGGGGTACCGCCACCATGGTGAGCAAGGGC-3' as forward and

5'- ACATGCATGCGCTTGTACAGCTCGTCCATGCC -3' as reverse;

Computational analysis of the mitochondria-targeting sequence in original Cameleon underlines the presence of a putative Kozak consensus sequence between the targeting sequence and the N-terminus of D3cpv. This sequence was removed and placed before the starting codon. Furthermore, we increased the number of amphiphilic amino acids in each of the four targeting sequences to improve the mitochondrial matrix import. The addition of the Kozak consensus sequence (GCCACC) and of the 33 aminoacids N-terminal sequence derived from COX VIII at 5', as well as the insertion of EcoRI and AgeI sites between CaM and M13 in 4mtD3cpv has been obtained by chemical synthesis (GeneArt Gene Synthesis service from Life Technology). In the mitochondria-targeted Cameleon obtained, mCerulean3 was amplified by PCR and substituted between BamHI and SphI sites, using specific primers:

5'-GCGGATCCGCCACCATGGTGAGCAAGGGC -3' as forward and

5'- ACATGCATGCGCTTGTACAGCTCGTCCATGCC -3' as reverse.

Glycines spacer addition between CaM and M13 was obtained by insertion of annealed oligonucleotides between EcoRI and AgeI restriction sites.

Oligonucleotides

5’-AATTCGTGCAGATGATGACCGCCAAGGGCGGCGGCGGCGGCGGCGGCGGCGGC
GGCGGCGGCGGCGGCGGCGGCGGCAGCAAGAGAAGATGGCAGAAAA-3’ (Forward),
and
3’CCGGTTTTCTGCCATCTTCTCTTGCTGCCGCCGCCGCCGCCGCCGCCGCCGCCGC
CGCCGCCGCCGCCGCCGCCCTTGGCGGTCATCATCTGCACG-5’ (Reverse)
were synthesized by Invitrogen.

For protein purification, D3cpv and D3mC3+16 cDNAs have been cloned in the E. coli expression vector pQE30 (QIAGEN) between KpnI/ HindIII restriction sites.

For AAV9 generation, D3mC3+16 and 4mtD3mC3+16 cDNAs were cloned in pAAV between BamHI and HindIII sites; D3mC3+16 and 4mtD3mC3+16 cDNAs were cloned in pAAV-Syn between HindIII and KpnI restriction sites. pAAV-Syn-ChR2(H134R)-GFP was a gift from Edward Boyden (Boyden et al., 2005, Addgene plasmid # 58880).

4mt-mCerulean3 has been amplified by PCR from 4mtD3mCerluean3-pcDNA3, using the following primers:

forward, 5’-ATGGTACCGCCACCATGAGCGTG-3’;

reverse 5’-GGCATGGACGAGCTGTACAAGTAACTCGAGCA-3’.

The PCR product was then cloned in pcDNA3 between KpnI/XhoI sites.

cpV has been amplified by PCR from 4mtD3mCerluean3, using the following primers:

forward, 5’-CGCGGATCCATGGATGGCGGAGTC-3’;

reverse 5’-CACAATATCGAGTAACTCGAGCGG-3’.

The PCR product was then cloned in pcDNA3 between BamHI/XhoI sites for cpV, or in 4mtD3mC3-pcDNA3 between BamHI/XhoI to get 4mt-cpV. 4mt-ECFP and ECFP in pcDNA3 were previously generated.

The Nucleotides and aminoacids sequence of the mCerulean3-based Cameleons is provided in Figure1- Table Supplement 9

AAV production

Recombinant AAV vectors used in this study were prepared by the AAV Vector Unit at the International Centre for Genetic Engineering and Biotechnology Trieste (http://www.icgeb.org/avu-core-facility.html), as described previously (Arsic et al., 2004) with a few modifications. Briefly, infectious recombinant AAV vector particles were generated in HEK293T cells culture in roller bottles by a cross-packaging approach whereby the vector genome was packaged into AAV capsid

serotype-9 (Inagaki et al., 2006). Viral stocks were obtained by PEG precipitation and $CsCl_2$ gradient centrifugation (Ayuso et al., 2010). The physical titer of recombinant AAVs was determined by quantifying vector genomes (vg) packaged into viral particles, by real-time PCR against a standard curve of a plasmid containing the vector genome (Zentilin et al., 2001); values obtained were in the range of $1x10^{12}$ to $1x10^{13}$ vg per milliliter.

Immunocytochemistry

Cells were fixed in Phosphate Buffered Saline (PBS) containing 4% paraformaldehyde (supplemented with sucrose 20% for cortical neurons) for 15 min, incubated with 50 mM NH_4Cl for 20 min, permeabilized with 0.1% Triton X-100 in PBS for 3 min and then blocked with 2% BSA and 0.2% gelatin for 30 min; mitochondria were stained using anti-TOM20 antibody (Santa Cruz Biotechnology, Dallas Texas, USA; 1:100, rabbit); neuronal cells using anti-NF200 (N5389, mouse Sigma-Aldrich Saint Louis, MI) and non-neuronal cells with anti-GFAP (Z0334 Dako, 14 New Bond St Bath BA1 1BE United Kingdom rabbit). Alexa Fluor 555 conjugated goat anti-rabbit or anti-mouse (Molecular Probes Invitrogen, Eugene) was applied for 1 hour at room temperature. Coverslips were mounted using Mowiol (Sigma-Aldrich Saint Louis, MI). Images were collected at Leica TCS SP5 II confocal system, equipped with a PlanApo 100×, numerical aperture 1.4 objective. For all images, pinhole was set to 1 Airy unit. The Argon laser line (488 nm) was used to excite FPs of the Cameleon sensors and the He/Ne 543 nm laser was used to excite the AlexaFluor555 antibody. Confocal microscopy imaging was performed at 1024×1024 pixels per image, with a 200 Hz acquisition rate. Images were elaborated with ImageJ program (Wayne Rasband, Bethesda, USA).

Immunohistochemistry

Brain slices cut from the infected hemisphere were fixed in 4% paraformaldehyde (PFA) in Tris-buffer saline, TBS: NaCl (150 mM), Tris (50 mM), pH adjusted to 7.4. For staining, floating slices were selected over a range of 400 μm. First, slices were washed in TBS and incubated in blocking buffer containing 0.3% TritonX-100 and 5% goat serum in TBS for 1 hour at room temperature (RT). Next, they were incubated overnight at 4°C with anti-TOM20 antibody (Santa Cruz Biotechnology, Dallas Texas, USA; 1:100, rabbit) and anti-NeuN (Millipore, 1:100, mouse). Then, slices were incubated for 1 hour at RT in the dark with goat anti-rabbit or anti-mouse Alexa555 (Molecular Probes Invitrogen, Eugene, 1:500). Mowiol-mounted slices were stored at 4°C until visualization by means of Leica TCS SP5 II confocal system as described above.

Confocal analysis of mCerulen3 fluorescence and mitochondrial targeting

HeLa cells expressing D3cpv/D3mC3 or 4mtD3cpv/4mtD3mC3 were fixed and then analyzed with Leica TCS SP5 II confocal system using the Ar/ArKr 458-nm laser line (ECFP/mCerulean3) and He/Ne 512-nm laser line (cpV). In order to compare the absolute fluorescence of ECFP and of mCerulean3, the measured intensity was normalized to the cpV recorded fluorescence, maintaining the recording parameters constant in subsequent acquisitions. Indeed, cpV is present in both probes, thus it was possible to use its fluorescence as a parameter to evaluate the protein expression level in each cell analyzed. Confocal microscopy imaging was performed as reported above.

To evaluate the targeting efficiency between old (29 aminoacids) and optimized (33 aminoacids) mitochondria-targeting sequence, six different fields have been acquired for each condition. The average ratio between the number of cells showing the proper mitochondrial localization of the probe and the total number of cells per field expressing the probes has been calculated.

Fluorescence microscope settings for FRET experiments

Live cells expressing the fluorescent probes were analyzed using a DM6000 inverted microscope (Leica, Wetzlar, Germany) with a 40× oil objective (HCX Plan Apo, NA 1.25). Excitation light produced by a 410 nm LED (#LZ1-00UA00, LED Engin) was filtered at the appropriate wavelength (425 nm) through a band pass filter, and the emitted light was collected through a beam splitter (OES s.r.l., Padua, Italy; emission filters HQ 480/40M (for ECFP) and HQ 535/30M (for cpV; dichroic mirror 515 DCXR). All filters and dichroic optics were from Chroma Technologies (Bellow Falls, VT, USA). Images were acquired using an IM 1.4C cool camera (Jenoptik Optical Systems) attached to a 12-bit frame grabber. Synchronization of the excitation source and the cool camera was performed through a control unit run by a custom-made software package, Roboscope (developed by Catalin Dacian Ciubotaru at VIMM, Padua, Italy). Exposure time varied from 100 ms to 200 ms, depending on the intensity of the fluorescent signal of the cells analyzed. Frequency of image capture depends on the speed of fluorescence changes we were detecting: usually images are acquired every 2-3 seconds, with the only exception of photostability experiments in which 1 image per second was acquired.

During the experiment, cells were mounted into an open-topped chamber and maintained in the proper medium. The extracellular-like medium (EC) is composed by modified Krebs-Ringer Buffer, mKRB; in mM: 135 NaCl, 5 KCl, 1 $MgCl_2$, 0.4 KH_2PO_4, 1 $MgSO_4$, 20 HEPES, 11 glucose, pH 7.4 at 37°C (or at 22°C for FLIM experiments), while intracellular-like medium contains in mM: 130 KCl, 10 NaCl, 1 $MgCl_2$, 2 succinic acid and 20 HEPES, pH 7.0 or 7.5 at 37°C (or at 22°C for FLIM

experiments). To evaluate pH sensitivity, titration and dynamic range of the probe in mitochondria, a modified intracellular-like medium (IC, see above) deprived of energy sources (succinic acid was not present) has been used. HEPES was substituted with 20 mM Tris to get pH 8.0 at 37°C or 22°C for FLIM experiment.

All media were perfused through a temperature controller (Warner Instruments, TC-324B) to maintain a temperature of 37°C in the chamber. Pre-incubations were also performed at 37°C.

Functionality experiments: classical experiments started in EC containing 1 mM $CaCl_2$; after perfusion with 600 µM EGTA (ethylene glycol tetraacetic acid), cells were stimulated by perfusion with 100 µM histamine (or ATP for MEFs cells).

Dynamic range: in HeLa cells expressing mitochondrial probes, minimal and maximal FRET conditions have been obtained as described above. In HeLa cells expressing cytosolic probes, cells permeabilization have been obtained by perfusing low amount of digitonin (5 µM) in Ca^{2+}-free medium containing 600 µM EGTA for 30 seconds, whereas for HeLa cells expressing mitochondrial probes, cells permeabilization have been obtained by perfusing digitonin (100 µM) in Ca^{2+}-free medium containing 600 µM EGTA for 30 seconds.

DR has been calculated dividing maximal ratio (cpV/ECFP or cpV/mCerulean3 fluorescence intensity at saturated [Ca^{2+}]) by minimal ratio (cpV/ECFP or cpV/mCerulean3 fluorescence intensity in Ca^{2+}-free medium containing 600 µM EGTA).

Photostability experiments: HeLa cells expressing different variants of cytosolic or mitochondrial probes were illuminated every second using the same laser intensity at 410 nm; images were acquired for 20 min in three different FRET conditions. For cytosolic Cameleon probes we analyzed: minimal FRET, obtained in EC containing 5 µM Ca^{2+} chelator BAPTA (1,2-bis(2-aminophenoxy)ethane-N,N,N'N'-tetraacetic acid)-AM; basal FRET, obtained in EC medium supplied with the physiological 1 mM [Ca^{2+}]. For mitochondrial Cameleon probes, after permeabilization with 100 µM digitonin, we analyzed: minimal FRET, obtained incubating permeabilized cells in IC Ca^{2+}-free medium containing 600 µM EGTA; basal FRET, obtained incubating cells in EC in the presence of physiological 1 mM $CaCl_2$. In FRET-based biosensors, illumination of the donor FP has a complex effect on the fluorescence emitted by each of the two chromophores. Indeed, the acceptor bleaching (due to FRET) upon excitation of the donor results in a reduction of its emitted light that is also proportional to the extent of FRET (and thus of the [Ca^{2+}]). On the contrary, the donor bleaching results in reduction of the donor fluorescence, while acceptor bleaching causes donor de-quenching. The latter, in turn,

causes a paradoxical increase in donor fluorescence. Accordingly, rather than the changes in the single fluorophore emission intensity, the parameter we evaluated is the change in the ratio, R, between the emission intensities at the two fluorophores peaks, at different Ca^{2+} concentrations.

In situ titration: HeLa cells expressing D3cpv, D3mC3+16, 4mtD3mC3 or 4mtD3mC3+16 were permeabilized with 5 (for cytosolic probes) or 100 (for mitochondrial probes) µM digitonin in IC Ca^{2+}-free medium containing 600 µM EGTA for 30 seconds and then incubated in the same medium without digitonin. Cells were then perfused with a IC (at pH 7.0 for cytosolic probes and at pH 7, 7.5 or 8 for mitochondrial probes) containing known Ca^{2+} concentrations, supplemented with 5 µM FCCP [Carbonyl cyanide-4-(trifluoromethoxy) phenylhydrazone] for mitochondrial probes titration. At the end of each experiment, saturating $CaCl_2$ concentration (5 mM) was applied. Data are presented as R%. IC supplied with 500 µM BAPTA free acid (Molecular Probes, Life Technology) has been used to achieve $[Ca^{2+}] < 1$ µM for K_d evaluation for mitochondrial calibration, whereas a Ca^{2+}-buffer solution was prepared by adding to the intracellular medium H-EDTA and EGTA (2 mM) for cytosolic probe calibration. The free $[Ca^{2+}]$ was estimated by MaxChelator2.5 and checked by fluorimetric measurements with Fura-2.

The data obtained are plotted as $\log_{10}[Ca^{2+}]$ (x-axis) and R% (y-axis) and fitted using Origin 8 SR5 (OriginLab Corporation). Fitting was performed using the Hill equation sigmoidal fitting (Palmer et al., 2004).

Mitochondrial Cameleon ratio-pH sensitivity: to evaluate changes in R upon mitochondrial pH acidification, HeLa cells expressing mitochondrial Cameleon probes have been perfused with EC supplemented with 1 mM $CaCl_2$, to record the R at resting condition, and then with the same medium supplemented with FCCP 5 µM

Nigericin protocol to collapse mitochondrial ΔpH:

HeLa cells expressing 4mtD3cpv or 4mtD3mC3+16 has been perfused with K^+-based medium (in mM: 5 NaCl, 130 KCl, 2 $MgCl_2$, 3 $CaCl_2$, 10 HEPES, 11 glucose, pH 7.4 at 37°C). To collapse mitochondrial pH to that of the cytosol, 100 nM nigericin has been manually added. Data obtained are plotted as $\Delta R/R_0$, where R_0 is R calculated at pH 8 (in the absence of nigericin).

Nigericin clamp method:

HeLa cells expressing D3cpv or D3mC3+16 has been perfused with an EC supplemented with 1 mM $CaCl_2$. To superimpose pH 6.0, 6.5, 7.0 and 7.5 into the cytosol, cells were perfused with a K^+-based

medium (see above) at the reported pH and supplemented with 1mM $CaCl_2$ and 5 µM nigericin. Data obtained are plotted as $\Delta R/R_0$, where R_0 is R calculated at pH 7.0.

Infection and Ca^{2+} imaging in primary culture

- Neonatal cortical and hippocampal neurons

At 8 DIV, cells were infected with 10^{11} vg of AAV9-syn-D3cpv, AAV9-syn-4mtD3cpv, AAV9-syn-D3mC3+16 or AAV9-syn-4mD3mC3+16 and Ca^{2+} imaging was performed 72-96 hours after infection. To trigger mitochondrial and cytosolic Ca^{2+} rises, a typical experiment was performed as follows: after perfusion with extracellular-like medium (see below) containing 1 mM $CaCl_2$, neurons depolarization is triggered with K^+-based medium (see below), whereas neurons oscillations are triggered by picrotoxin 50 µM perfusion.

- Neonatal cardiomyocytes

Immediately after plating, cardiomyocytes have been infected with 10^{11} vg of AAV9-CMV-D3mC3+16 or AAV9-CMV-4mD3mC3+16. From DIV1, cells were maintained in DMEM/Medium 199 (4:1) medium containing 5% horse serum and 0.5% newborn calf serum for 3 days. Experiments were carried out 96 hours after infection.

- Differentiation of iPSC into CMs.

At day 7, cardiomyocytes have been infected with 10^{11} vg of AAV9-CMV-D3mC3+16 or AAV9-CMV-4mD3mC3+16. Experiments were carried out 96 hours after infection.

Spontaneous Ca^{2+} oscillations have been measured in extracellular-like medium (see below) containing 2 mM $CaCl_2$.

Buffer titration with spectrofluorometer

To evaluate $[Ca^{2+}]$ in IC medium used for the titration experiments in IC containing BAPTA free acid, 0.5 µM of Fura-2 (Fura-2 Pentapotassium salt, Molecular Probes) was added to the solution and fluorescence evaluated using the Perkin Elmer LS50B spectrofluorometer equipped with magnetic stirring (340 and 380 excitation intensity, 510 nm emission) at 37°C.

$[Ca^{2+}]$ concentration was calculated as: $[Ca^{2+}]_{free} = 224^* Q [(R-R_{min})/(R_{max}-R)]$, where 224 nM is the Fura-2 K_d, R represents the fluorescence intensity ratio $F_{\lambda1}/F_{\lambda2}$, in which λ_1 (~340 nm) and λ_2 (~380 nm) respectively. R corresponding to the titration end points is denoted by the subscripts indicating the minimum and maximum Ca^{2+} concentration. Q is the ratio of F_{min} to F_{max} at λ_2 (~380 nm).

Aequorin Ca^{2+} Measurements

MEF or HeLa cells (0.5×10^5) were plated on coverslips (13-mm diameter), after 24 h were transfected and used for Ca^{2+} measurements the day after transfection. Cells were incubated at 37°C with coelenterazine (5 µM) for 1 h in an EC (see above) and then transferred to the perfusion chamber. All the luminescence measurements were carried out at 37°C. The experiments were terminated by cell permeabilization with digitonin (100 µM) in a hypotonic Ca^{2+}-rich solution (10 mM $CaCl_2$ in H_2O) to discharge the remaining unused aequorin pool. The light signal was collected as previously described (Brini et al., 1995). A typical experiment started in EC containing Ca^{2+} 1 mM, after 1 minute the Ca^{2+} outside is removed perfusing EC containing EGTA 0.6 mM. In all the Ca^{2+} experiments maximal effective doses of the stimuli (ATP 100 µM, Histamine100 µM) were used.

mtGCaMP6f imaging

Neonatal rat cardiomyocytes transfected with mtGCaMP6f or mt-GFP cells with TransFectin™ Lipid Reagent (Bio-Rad Laboratories) were analyzed using a DM6000 inverted microscope (Leica) with a 40X oil objective (HCX Plan Apo, NA 1.25) as described above. Excitation light produced by a 460 nm LED (LZ1-10DB05, LED Engin) was filtered at 470 nm through an excitation filter (ET470/24), and the emitted light was collected through a long pass filter 515 nm and a dichroic mirror 510 DCXR. Cells were mounted in an open-topped chamber thermostated at 37°C and maintained in an EC containing 2 mM $CaCl_2$.

Western Blot

HeLa cells expressing D3cpv, 4mtD3cpv, D3mC3+16 or 4mtD3mC3+16 were lysed in RIPA buffer (50 mM Tris, 150 mM NaCl, 1% Triton X-100, 0.5% deoxycholic acid, 0.1% SDS, protease inhibitor cocktail, pH 7.5) and incubated in ice for 30 min. Insolubilized material was spun down at 4000 x g for 5 min at 4°C. 35 µg of protein was loaded onto polyacrylamide gels (10-12%) and immunoblotted. Proteins were resolved by TruPAGE™ Precast Gels 4-12% (Sigma-Aldrich Saint Louis, MI) in TruPAGE™ TEA-Tricine SDS Running Buffer (Sigma-Aldrich Saint Louis, MI), blotted onto a nitrocellulose membrane and probed with α-GFP antibody (Rabbit monoclonal; Cell signaling technology, 1:1000).

FLIM

FLIM measurements were carried out using the time-correlated single-photon counting (TCSPC) method. The experimental apparatus is based on a scanning confocal microscope (Olympus FV300, IX-71) coupled with a PicoHarp 300 TCSPC electronics (PicoQuant) and two single-photon counting avalanche photodiodes (SPAD, MPD, Italy). Excitation was provided by a frequency doubled

Ti:Sapphire fs laser system (Coherent, Mira900-F, 400 nm, 76 MHz), focused onto the sample using a 60× water immersion microscope objective. The laser power on the sample is typically around 50-200 μW. The scan area dimension was selected on the microscope software in order to map few cells in each analysis. The acquisition time was set to 3-5 minutes to collect around 10^4 counts in the peak channel. All experiments were conducted at room temperature at 22 °C.

The fluorescence signal was split in two channels by a 40/60% beam-splitter for the detection of donor emission (Semrock, 482/25 bandpass filter) and of mainly acceptor fluorescence (Semrock, 542/25 bandpass filter). The data acquisition was performed in reverse start-stop mode, with each detected photon assigned to one of the 820 channels with 16 ps width. Lifetime decays, extracted from the signals collected on a selected ROI containing a single cell, were analyzed with the Symphotime software (PicoQuant), using a model with increasing number of exponential terms until no significant improvement of the fit quality is obtained. For each measurement session, the residual autofluorescence signal has been used for the calculation of the instrumental response function (IRF) for both detection channels. Its FWHM (Full width at half maximum), calculated with the IRF reconstruction script of the Symphotime software, was typically 150-200 ps. An intensity threshold of 100 counts was set in order to reduce the autofluorescence contribution to the overall FLIM fluorescence intensity. The FLIM analysis was then performed using a pixel-by-pixel n-exponential reconvolution fit procedure.

For multi-exponential decays, we have calculated the amplitude-weighted average lifetime as: $\langle\tau\rangle = \sum_i A_i \tau_i$, where A_i, with $i = 1, ..., n$, are the amplitudes of the n decay time components at t=0 ($\sum_i A_i = 1$), τ_i are the decay times. Since the amplitude-weighted lifetime value is proportional to the area under the decay curve, which is proportional to the steady-state fluorescence intensity that would be measured in the same experimental conditions, $\langle\tau\rangle$ is the most-accurate parameter for the FLIM-FRET analysis. Indeed, the FRET efficiency is defined as:

$$E_{FRET} = 1 - \frac{F_{DA}}{F_D} = 1 - \frac{\int I_{DA}(t)dt}{\int I_D(t)dt}$$

F_{DA} and F_D are respectively the emission intensity of the donor in presence or in absence of the acceptor. If the donor has a mono-exponential decay in both conditions, the FRET efficiency can be expressed as: $E_{FRET}^{1exp} = 1 - \frac{\tau_{DA}}{\tau_D}$, where τ_{DA} and τ_D are the fluorescence lifetime in presence or in

absence of acceptor moiety. In all other cases, *i.e.* when the decay curve requires a multi-exponential fitting model, the efficiency can be calculated as: $E_{FRET}^{n_{exp}} = 1 - \frac{\langle \tau_{DA} \rangle}{\langle \tau_D \rangle}$ (Grailhe et al., 2006; Sun et al., 2011).

Rise term analysis for pH effect on lifetime

Since both acidification and increase in [Ca^{2+}] exert qualitatively the same effect on average donor lifetime, we sought for a parameter to discriminate between pH and Ca^{2+} effects. Based on previously published work (Borst et al., 2008), we employed the "rise" term analysis on the acceptor decay curve. The rise term reflects the delay in acceptor emission decay due to indirect excitation from donor emission and it is represented by a negative amplitude contribution to the acceptor emission decay.

mt-SypHer

Mitochondrial matrix pH was monitored in HeLa cells transfected with MCU, MICU1, MCU and MICU1 or void vector in the presence of mt-SypHer. Fluorescence was visualized using an inverted microscope (Zeiss Axiovert 100) with a 40× oil objective (Fluar, NA 1.30). Excitation light at 480±7.5 nm and 430±7.5 nm was produced by a monochromator (polychrome V; TILL Photonics) and passed through an emission filter 535RDF45 and a dichroic mirror (505 DCXRU). Images were acquired using a cooled CCD camera (SensicamQE PCO, Kelheim, Germany). All filters and dichroic mirrors were from Chroma Technologies (Bellow Falls, VT, USA). Images were acquired very 10 s with 100 ms exposure. The classical protocol consists in perfusion with different solutions at RT: extracellular-like medium (R_{basal}), cells permeabilization for 1 min in intracellular-like medium at pH 6 in presence of FCCP, 1 min of intracellular-like medium at pH 6.0 (R_{min}) and 1 min of intracellular-like medium at pH 9.0 (R_{max}). Data are presented as $[(R_{basal}-R_{min})/(R_{max}/R_{min})]*100$, where R is calculated as F480/530.

Two-photon spectroscopy

To measure the two-photon excitation spectra we expressed mCerulean3 and cpV in HeLa cells. Fluorescence was imaged with a multiphoton Imaging System (Scientifica Ltd., Uckfield, East Sussex, United Kingdom) equipped with a 20X water immersion objective (1 NA, Olympus). Excitation was provided by a pulsed infrared laser (Chameleon Ultra 2, Coherent, Santa Clara, CA). Excitation power at the sample (Pw) was measured with a powermeter (Thorlabs), and controlled

during the acquisition by means of a Pockel Cell (Conoptics model 302 RM) in order to maintain a constant photon number (n_φ) impinging on the sample at all wavelengths (λ): $n_\varphi \propto Pw \cdot \lambda$.

AAV9 injection

Mice used were C57Bl/6 littermates.

For experiments in adult cardiomyocytes: 3 months-old mice have been injected in the tail vein. Cardiomyocytes isolation have been performed 6 months after injections. Vector solution was drawn into a 3/10 cc 30 gauge insulin syringe. Virus injections were in a total volume of 100 µl of PBS and a total of 10^{11} vg of AAV9-CMV-mCerulean3- based Cameleon probes were injected.

For somatosensory cortex brain slices experiments: P0-P2 pups were anaesthetized by hypothermia and secured into a modeled platform. Then, viral vectors (diluted to 50 % in PBS, final volume injected 0.25 µl, $1.25x10^7$ vg injected) were pressure-injected by using a pulled glass pipette. Two weeks after the injection, somatosensory cortex brain slices were prepared to perform imaging experiments.

For hippocampal brain slices experiments: P30 mice were anaesthetized with isoflurane (4% for induction and 2% for maintenance). Depth of anesthesia was assured by monitoring respiration rate and reactions to pinching the tail and toe. Viral vectors (2 µl, $1.25x10^7$ vg injected) were injected unilaterally using a pulled glass pipette in conjunction with a custom-made pressure injection system (–2 mm posterior to Bregma, 1.6 mm lateral to sagittal sinus, and 1.8 mm depth). After injections, the skin was sutured, mice were revitalized under a heat lamp and returned to their cage. Two weeks after the injection, hippocampal brain slices were prepared to perform imaging experiments.

For *in vivo* experiments: 2 months-old mice were anaesthetized with Zoletil (30 mg/kg, Virbac, Cedex, France) and Xilazyne (20 mg/kg, BIO98 srl, Barcelona, Spain). Eyelid reflex and reactions to pinching the tail and toe were used to monitor depth of anesthesia. After drilling two holes into the skull over the somatosensory cortex (from Bregma 0-1.5 mm AP, 1.5 mm ML, 150 µm depth), the viral vectors (diluted to 50 % in PBS; final volume injected per hole,1 µl; $5x10^7$ vg injected) were pressure-injected through a pulled glass pipette. *In vivo* imaging experiments through a cranial window were has performed 2-3 weeks after injection.

Isolation of adult mouse ventricular myocytes.

Adult mouse ventricular myocytes were isolated from hearts of 9 months old C57Bl6/J mice. In brief, mice were injected intraperitoneal (i.p.) with 1,000 U heparin 30 min before the isolation procedure to prevent coagulation of blood in the arteries. Hearts were quickly excised and retrogradely perfused

at 37˚C for 2 min with Ca^{2+}-free perfusion buffer (PB, in mM: NaCl 120, KCl 14.75, KH_2PO_4 0.6, Na_2HPO_4 0.3, $MgSO_4$ 1.2, HEPES 10, $NaHCO_3$ 4.6, taurine 30, BDM 10, glucose 5.5, pH 7.4). Collagenase type II (1.2 mg/ml, Worthington) and protease type XIV (0.05 mg/ml, Sigma-Aldrich, Saint Louis, MI) were added to the PB and hearts perfused for 3 min at 2 ml/min and then for 8 min at 1.5 ml/min. After digestion, hearts were placed in 10 ml of PB, cut into smaller pieces and cardiomyocytes dissociated by gentle pipetting. The suspension was filtered through 100 µm mesh, centrifuged at 500 g for 1 min and resuspended in PB containing 5 mg/ml BSA and 125 µM $CaCl_2$. After the myocytes were separated by gravity for ~10 min, the supernatant was aspirated and myocytes resuspended in Tyrode's solution (in mM: 140 NaCl, 10 HEPES, 1 $MgCl_2$, 5 KCl; and glucose, 1 mg/ml) added with 250 µM Ca^{2+}. Ca^{2+} concentration was increased gradually and the final cell pellet was suspended in 1.8 mM Ca^{2+}. All solutions were adjusted to pH 7.4 with NaOH.

Brain Slice Preparation

1- Somatosensory cortex slices

Coronal slices of 350 µm containing somatosensory cortex were obtained from P15-P20 mice. Animals were anaesthetized with Zoletil (30 mg/kg, Virbac, Cedex, France) and Xilazyne (20 mg/kg, BIO98 srl, Barcelona, Spain) and the brain was removed and transferred into an ice-cold standard solution (in mM: 125 NaCl, 2.5 KCl, 2 $CaCl_2$, 1 $MgCl_2$, 25 glucose, pH 7.4 with 95% O_2, and 5% CO_2). Coronal slices were cut with a vibratome (Leica Vibratome VT1000S Mannheim, Germany) in the ice-cold solution described in (Dugue et al., 2005). Slices were transferred for 1 min in a solution at RT containing (in mM): 225 D-mannitol, 2.5 KCl, 1.25 NaH_2PO_4, 26 $NaHCO_3$, 25 glucose, 0.8 $CaCl_2$, 8 $MgCl_2$, 2 kynurenic acid with 95% O_2, and 5% CO_2. Slices were transferred in standard solution at 30°C for 20 min and then maintained at RT for the entire experiment.

2- Hippocampal slices

P45 mice were deeply anesthetized with Zoletil (30 mg/kg, Virbac, Cedex, France) and Xilazyne (20 mg/kg, BIO98 srl, Barcelona, Spain) and perfused intracardially with 10 ml of ice-cold cutting solution (sucrose based low Ca^{2+} ACSF containing in mM: 203 sucrose, 3 KCl, 2 $MgCl_2$, 0.5 $CaCl_2$, 2 $NaCO_3$, 1.5 Na_2HPO_4, 25 glucose). The brain was rapidly removed and 350 µm coronal slices were cut with a vibratome (Leica Vibratome VT1200S Mannheim, Germany) in the ice-cold cutting solution. Slices were then transferred in standard ACSF solution at 30°C for 30 min and then maintained at RT for the entire experiment.

Brain Slice Imaging Experiments

Slice imaging experiments were conducted with a two-photon laser scanning microscope Multiphoton Imaging System (ScientifiCaLtd., Uckfield, East Sussex, United Kingdom) equipped with a pulsed infrared laser (Chameleon Ultra 2, Coherent, Santa Clara, CA; laser repetition rate 80 MHz). The excitation wavelength used was 800 nm. Power at sample was controlled in the range 5–10 mW. Images were acquired at a resolution of 512×512 pixels at 1.53 Hz frame rate. Imaging was performed in cortical layers II–III or in hippocampus and conducted at maximum for 1 hour with 1–2 minutes recording sessions every 5 min.

***In vivo* Imaging Experiments**

Mice were anaesthetized with an intraperitoneal injection of Zoletil (30 mg/kg, Virbac, Cedex, France) and Xilazyne (20 mg/kg, BIO98 srl, Barcelona, Spain) solved in saline solution. Animal pinch withdrawal and eyelid reflex were tested to assay the depth of anesthesia. Atropine (0.07 mg/kg body weight) was injected subcutaneously to avoid saliva accumulation. Body temperature was maintained at 37°C with a feedback-regulated heating pad. Respiration rate, heart rate and core body temperature were monitored throughout the experiment. The mouse was head-fixed and a craniotomy of 2–3 mm in diameter was drilled over the somatosensory cortex. The dura was carefully removed and the craniotomy was immediately covered with a coverslip with a hole. Warm HEPES-buffered artificial cerebrospinal fluid filled the chamber to prevent desiccation and maintain ionic balance. To perform topical application of NMDA, a borosilicate micropipette was positioned over the hole on the coverslip. Imaging was performed with a two-photon microscope (Ultima IV, Prairie Technology now Bruker, USA) at 800 nm with a Chameleon 2 laser (see above). Imaging was performed at a resolution of 256×256 pixels (around 150 μm below the cortical surface) and acquired at 2 Hz.

Stimuli application in Ca^{2+} imaging experiments

KCl (30 mM) in iso-osmotic extracellular-like medium was bath-applied for cotical neurons and somatosensory cortex slices, as well as NMDA (50 μM), DHPG (50 μM) and CCH (500μM) were perfused in experiments with hippocampal slices or picrotoxin (50 μM) in hippocampal and cortical neurons. NMDA 1 mM and D-serine 20 μM or NMDA 1 mM only have been applied by means of a pressure ejection unit (PDES, NPI Electronics, Tamm, Germany) connected to a glass pipette (tip diameter 2–3 μm) for somatosensory cortex brain slices or for *in vivo* experiments.

Quantification and statistical analysis

Off-line analysis of FRET experiments was performed with ImageJ software (National Institutes of Health). cpV and ECFP/mCerulean3 images were subtracted of background signals and distinctly analyzed after selecting proper regions of interest (ROIs) on each cell; subsequently, a ratio between cpV and ECFP (or mCerulean3) emissions was calculated ($R=F_{530}/F_{430}$).

Data are presented as a normalized $\Delta R/R_0$, where R_0 is the R value at the beginning of the experiment (t_0) and ΔR is the R value at each time (t) of the experiment minus R_0, or as R%, calculated as: $R\%= (R-R_{min})/R_{max}-R_{min})x100$.

All data are representative of at least three different experiments. Unless otherwise stated, numerical values presented throughout the text refer to mean±SEM (N = number of independent experiments or cells). Statistical significance ($p < 0.05$) was detected by Student's t test (two-sided) for two groups' comparison with normal distribution, Wilcoxon test for comparison between two groups with non-normal distribution or one-way ANOVA for comparison among three different groups.

The ratiometric video was generated by an experiment carried out with a NIKON Eclipse Ti fluorescence microscope and the imaging analysis system provided by the company (NIS software). The images were pseudo-colored using a rainbow-like look-up table where low and high ratio values are represented by blue and red, respectively.

Key resources table

REAGENT or RESOURCE	SOURCE	IDENTIFIER
Antibodies		
anti-TOM20	Santa Cruz Biotechnology	sc-11415
anti-NF200	Sigma-Aldrich	N5389
anti-GFAP	Dako	Z0334
Alexa Fluor 555 conjugated goat anti-rabbit	Molecular Probes Invitrogen	A27039
Alexa Fluor 555 conjugated goat anti-mouse	Molecular Probes Invitrogen	A28180
anti-NeuN	Millipore	MAB377
Chemicals, Peptides, and Recombinant Proteins		
Mowiol	Sigma-Aldrich	81381
Histamine	Sigma-Aldrich	H7250
ATP	Sigma-Aldrich	A1852
FCCP	Sigma-Aldrich	C2920
Nigericin	Sigma-Aldrich	N7143
Fura 2 Free Acid	Thermo Fisher Scientific	F-1200
Coelenterazina	Biotium	10110
NMDA	Sigma-Aldrich	M3262
DHPG	Sigma-Aldrich	D3689
CCH	Sigma-Aldrich	C4382
Picrotoxin	Sigma-Aldrich	P1675
BAPTA	Sigma-Aldrich	14513
Experimental Models: Cell Lines		
HeLa	ATCC	CCL2
MEF (C57BL/6)	ATCC	SCRC-1008
Experimental Models: Organisms/Strains		

Mice	Charles River Labs	C57BL6J
Software and Algorithms		
OriginPro	OriginLab	https://www.originlab.com/Origin
ImageJ	Wayne Rasband, Bethesda, USA	https://imagej.nih.gov/ij/
Roboscope	Catalin Dacian Ciubotaru at VIMM, Padua, Italy	

References

Arsic, N., Zacchigna, S., Zentilin, L., Ramirez-Correa, G., Pattarini, L., Salvi, A., Sinagra, G., and Giacca, M. (2004). Vascular endothelial growth factor stimulates skeletal muscle regeneration *in vivo*. Mol Ther *10*, 844-854.

Ayuso, E., Mingozzi, F., Montane, J., Leon, X., Anguela, X.M., Haurigot, V., Edmonson, S.A., Africa, L., Zhou, S., High, K.A., *et al.* (2010). High AAV vector purity results in serotype- and tissue-independent enhancement of transduction efficiency. Gene Ther *17*, 503-510.

Borst, J.W., Laptenok, S.P., Westphal, A.H., Kuhnemuth, R., Hornen, H., Visser, N.V., Kalinin, S., Aker, J., van Hoek, A., Seidel, C.A., *et al.* (2008). Structural changes of yellow Cameleon domains observed by quantitative FRET analysis and polarized fluorescence correlation spectroscopy. Biophys J *95*, 5399-5411.

Boyden, E.S., Zhang, F., Bamberg, E., Nagel, G., and Deisseroth, K. (2005). Millisecond-timescale, genetically targeted optical control of neural activity. Nat Neurosci *8*, 1263-1268.

Brini M, Marsault R, Bastianutto C, Alvarez J, Pozzan T, Rizzuto R.(1998). Transfected aequorin in the measurement of cytosolic Ca2+ concentration ([Ca2+]c). A critical evaluation. J Biol Chem. **1995** Apr 28;270(17):9896-903.

Dugue, G.P., Dumoulin, A., Triller, A., and Dieudonne, S. (2005). Target-dependent use of co-released inhibitory transmitters at central synapses. J Neurosci *25*, 6490-6498.

Grailhe, R., Merola, F., Ridard, J., Couvignou, S., Le Poupon, C., Changeux, J.P., and Laguitton-Pasquier, H. (2006). Monitoring protein interactions in the living cell through the fluorescence decays of the cyan fluorescent protein. Chemphyschem *7*, 1442-1454.

Inagaki, K., Fuess, S., Storm, T.A., Gibson, G.A., McTiernan, C.F., Kay, M.A., and Nakai, H. (2006). Robust systemic transduction with AAV9 vectors in mice: efficient global cardiac gene transfer superior to that of AAV8. Mol Ther *14*, 45-53.

Palmer, A.E., Jin, C., Reed, J.C., and Tsien, R.Y. (2004). Bcl-2-mediated alterations in endoplasmic reticulum Ca2+ analyzed with an improved genetically encoded fluorescent sensor. P Natl Acad Sci USA *101*, 17404-17409.

Rink TJ, Tsien RY, Pozzan T. (1982). Cytoplasmic pH and free Mg2+ in lymphocytes. J Cell Biol. 1982 Oct;95(1):189-96.

Sun, Y., Day, R.N., and Periasamy, A. (2011). Investigating protein-protein interactions in living cells using fluorescence lifetime imaging microscopy. Nat Protoc *6*, 1324-1340.

Zentilin, L., Marcello, A., and Giacca, M. (2001). Involvement of cellular double-stranded DNA break binding proteins in processing of the recombinant adeno-associated virus genome. J Virol *75*, 12279-12287.